IRREGULAR WAVE SEEPAGE AND OVERTOPPING ON COBBLE BEACHES AND REVETMENTS

BY

FRANCISCO J. DE LOS SANTOS AND NOBUHISA KOBAYASHI

RESEARCH REPORT NO. CACR-06-01

CENTER FOR APPLIED COASTAL RESEARCH

Ocean Engineering Laboratory
University of Delaware
Newark, Delaware 19716

Experiments were conducted in a wave flume to investigate wave seepage and overtopping of permeable stone slopes with wide crests. The numerical model based on the time-averaged continuity, momentum and energy equations is extended to include the landward water flux due to wave seepage and overtopping. The measured wave runup distributions are fitted to the Weibull distribution whose shape parameter increases with the increase of the wave overtopping probability. The wave overtopping rate normalized by the wave-induced water flux at the still water shoreline is shown to depend on the wave overtopping probability and the horizontal number of stones above the maximum wave setup. A simple formula for the seepage rate is proposed by analyzing the seepage flow driven by the wave setup on the seaward slope. The extended numerical model is shown to be in agreement with the measurements of the free surface elevation, cross-shore velocity, wave runup, and seepage and overtopping rates but will need to be evaluated using more extensive data sets.

ACKNOWLEDGEMENTS

This study was partially supported by the U.S. Army Corps of Engineers, Coastal and Hydraulics Laboratory under Contract Number DACW42-03-C-0024. The first author was supported by a Scholarship from the Spanish Ministry of Education, F.P.U. AP20024082. The first author would like to thank his advisor, Prof. Miguel A. Losada, for all the encouragement and support during his Ph.D. study at the University of Granada, Spain.

TABLE OF CONTENTS

LIST OF FIGURES

LIST OF TABLES

CHAPTER 1 INTRODUCTION

Wave overtopping of a coastal structure is important in determining the required crest height of the structure. For a low-crested rubble-mount structure, it is necessary to predict the amount of water and wave energy transmitted through and over the porous structure (Zanuttigh and Lamberti 2006). Wave overtopping of a cobble beach may cause damage to landward structures (Allan and Komar 2002). As a result, a large number of laboratory experiments on wave overtopping were conducted (Steendam et al. 2004). Field measurements of wave overtopping rates were also performed (Troch et al. 2004). Nevertheless, the wave overtopping rate cannot be predicted accurately where the error may be as large as a factor of 10 for small overtopping rates (Pozueta et al. 2004). To improve our quantitative understanding of wave overtopping processes on porous structures, this study examines the effect of wave overtopping on the distribution of irregular wave runup, the seepage flow rate through a permeable slope, and the effect of infiltration on the wave overtopping rate where Verhagen et al. (2004) showed experimentally that infiltration on a wide crest was substantial.

First, experiments were conducted in a wave flume to measure the probability distribution of wave runup and the seepage and overtopping rates through and over permeable slopes with wide crests. Second, the time-averaged probabilistic model for predicting wave transmission over submerged porous structures (Kobayashi et al. 2006b) and wave runup on permeable slopes (Kobayashi et al. 2006a) is extended to allow the landward water flux due to seepage and overtopping. A Weibull distribution is fitted to the measured distribution of wave runup on the low-crested structure to predict the probability of wave overtopping P_o. The seepage flow driven by wave setup on the permeable slope is analyzed to obtain a formula for the seepage rate. The wave overtopping rate normalized by the wave-induced onshore water flux at the still water shoreline is expressed as a function of P_o where the infiltration width above the maximum wave setup is included in the formula. Third, the extended time-averaged probabilistic model is shown to predict the significant and 2% runup heights, seepage and overtopping rates and wave reflection coefficients fairly well. However, the extended model calibrated using the present experiments will need to be compared with additional experiments.

In the following, the experiments are presented first because the proposed formulas are based on the experimental observations. Second, the time-averaged model based on the continuity, momentum and energy equations is extended to predict the seepage and overtopping rates. Third, the time-averaged model and formulas are compared with the experiments. Finally, the findings of this study are summarized.

It is noted that the results in this report will be presented concisely by de los Santos, Kobayashi and Losada (2006) and Kobayashi and de los Santos (2006).

CHAPTER 2 EXPERIMENTS

Twenty two tests under incident irregular waves were conducted in a wave flume to investigate wave seepage and overtopping of permeable 1/5 slopes with wide crests. This chapter describes the experimental setup for the seepage (S) and overtopping and seepage (OS) tests and summarizes the overtopping (O) experiment conducted by Kobayashi and Raichle (1994) with a 1/2 slope stone revetment. The obtained data for all the three experiments are tabulated for the development and validation of the numerical model. Finally, the measured runup distribution is analyzed and fitted to a Weibull distribution to take into account the decrease of the runup due to wave overtopping.

2.1 EXPERIMENTAL SETUP

Experiments were conducted in a wave flume that was 33 m long, 0.6 m wide and 1.5 m high as shown in Fig. 1. An impermeable smooth beach with a 1/34.4 slope was installed in the flume. Angular stone was placed on a 1/5 impermeable slope to simulate an idealized cobble beach. The mass of individual stones was in the range of 66 – 160 g and the median mass was M_{50} = 118 g. The density and porosity of the stone were ρ_s = 2.95 g/cm^3 and n_p =

0.5, respectively. The nominal diameter, $D_{n50} = (M_{50}/\rho_s)^{1/3}$, was 3.4 cm. No stone movement occurred in these experiments. The vertical thickness of the stone layer was 14 cm. Irregular waves, based on the TMA spectrum, were generated using a piston-type wave paddle in a burst of 429.6 s for each test. The initial transient of 20 s in each burst was removed from the measured time series sampled at a rate of 20 Hz. The wavemaker was located in the still water depth $d_h = (d_t + 31)$ cm where the still water depth d_t at the toe of the 1/5 slope was varied from 20.5 cm to 24.5 cm.

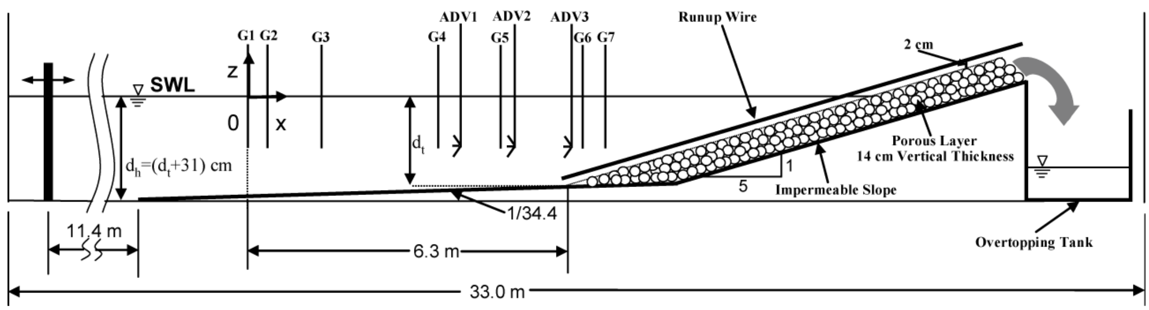

Fig. 1: Experimental setup for 1/5 permeable slope tests.

For each test, seven capacitance-type wave gauges and a runup wire were used to measure the time series of the free surface elevations above the still water level (SWL). The vertical height δ_r of the runup wire above the 1/5 slope was approximately 2 cm. Wave gauges 1 – 3 were located immediately outside the surf zone and used to separate the incident and reflected waves using linear wave theory (Kobayashi et al. 1990). The averaged reflection coefficient r is defined here as $r = (H_{rms})_r/(H_{rms})_i$ where $(H_{rms})_r$ and $(H_{rms})_i$ are the reflected and incident root-mean-square wave heights. The root-mean-square wave height H_{rms} is defined as $H_{rms} = \sqrt{8}\,\sigma_\eta$ with σ_η = standard deviation of the free surface elevation η. Wave gauges 4 – 7 measured the irregular breaking wave transformation. Three 3D acoustic Doppler velocimeters (ADV) were used to measure fluid velocities approximately in the mid depth below SWL. A tank was used to collect and measure the volume of seeped and overtopped water. The elevation of the tank edge above the toe of the 1/5 slope was 27.2 cm above SWL.

The crest geometry for 12 seepage tests is shown in the top panel of Fig. 2 where the crest height R_c = (39.1 – d_t) cm above SWL was so high that uprushing water on the permeable slope seeped and flowed into the tank with no or little overtopping over the crest. The measured seepage rates, q_s, were in the range of 0.04 – 5.57 cm^2/s, as shown in Table 1. To allow significant wave overtopping, the crest height R_c was reduced to R_c = (30.2 – d_t) cm by removing stones 3 cm above the tank edge as shown in the bottom panel of Fig. 2. The combined overtopping and seepage rates, q_{os}, for 10 tests were in the range of 0.11 – 12.56 cm^2/s. The flow rate into the tank for the same wave conditions increased by a factor of 2 – 3 due to the reduced crest height.

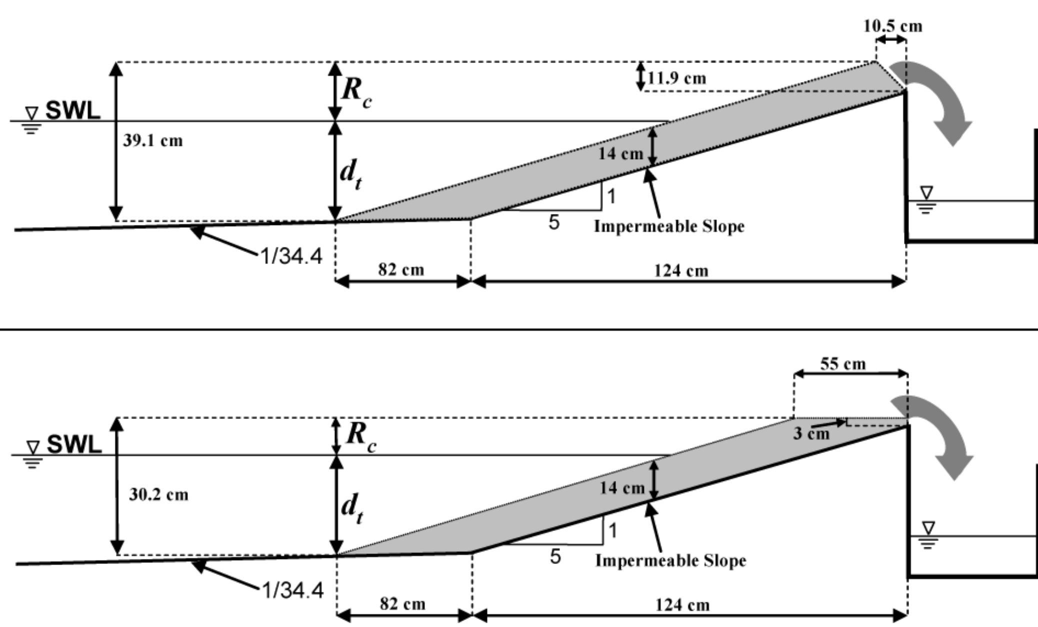

Fig. 2: Crest geometry for seepage tests (top) and overtopping and seepage tests (bottom).

Tables 1 and 2 summarize the wave conditions outside the surf zone for the seepage (S) tests and the overtopping and seepage (OS) tests where d_1, T_p and H_{rms} = water depth, spectral peak period and root-mean-square wave height measured at wave gauge 1, respectively. The wave reflection coefficient r was reduced only slightly due to the reduced crest height.

Table 1: Wave characteristics at wave gauge 1 for seepage (S) tests.

Test	d_1 [cm]	T_p [s]	H_{rms} [cm]	d_t [cm]	R_c [cm]	q_s [cm²/s]	r
RS20B1	38.9	2.3	11.2	20.6	18.6	0.12	0.20
RS20B2	38.9	2.3	11.2	20.6	18.6	0.10	0.20
RS20C1	38.9	3.0	7.3	20.6	18.6	0.04	0.23
RS20C2	38.9	3.0	7.3	20.6	18.6	0.05	0.23
RS22B1	40.9	2.3	11.6	22.6	16.6	1.57	0.20
RS22B2	40.9	2.3	11.6	22.6	16.6	1.13	0.20
RS22C1	40.9	2.9	7.6	22.6	16.6	0.31	0.23
RS22C2	40.9	2.9	7.6	22.6	16.6	0.30	0.23
RS24B1	42.9	2.3	11.9	24.6	14.6	5.57	0.20
RS24B2	42.9	2.3	11.9	24.6	14.6	5.02	0.20
RS24C1	42.9	2.9	7.8	24.6	14.6	2.23	0.23
RS24C2	42.9	2.9	7.8	24.6	14.6	1.84	0.23

d_1 =still water depth at wave gauge 1; T_p = spectral peak period; H_{rms} = root-mean-square wave height; d_t = toe depth; R_c = crest height; q_s = seepage rate; r = reflection coefficient.

Table 2: Wave characteristics at wave gauge 1 for overtopping and seepage (OS) tests.

Test	d_1 [cm]	T_p [s]	H_{rms} [cm]	d_t [cm]	R_c [cm]	q_{os} [cm²/s]	r
RO20B1	38.9	2.3	11.3	20.6	9.70	0.28	0.19
RO20C1	38.9	3.0	7.3	20.6	9.70	0.11	0.22
RO22B1	40.9	2.3	11.6	22.6	7.70	3.36	0.20
RO22B2	40.9	2.3	11.7	22.6	7.70	3.22	0.20
RO22C1	40.9	2.9	7.5	22.6	7.70	1.07	0.22
RO22C2	40.9	2.9	7.5	22.6	7.70	1.07	0.22
RO24B1	42.9	2.3	11.9	24.6	5.70	12.18	0.20
RO24B2	42.9	2.3	11.9	24.6	5.70	12.56	0.20
RO24C1	42.9	2.9	7.8	24.6	5.70	4.33	0.21
RO24C2	42.9	2.9	7.8	24.6	5.70	5.02	0.21

d_1 =still water depth at wave gauge 1; T_p = spectral peak period; H_{rms} = root-mean-square wave height; d_t = toe depth; R_c = crest height; q_{os} = combined overtopping seepage rate; r = reflection coefficient.

Table 3 summarizes the wave characteristics at wave gauge 1 for the wave overtopping (O) tests by Kobayashi and Raichle (1994). For these tests no seepage flow occurred. Fig. 3 shows their experimental setup for a revetment where a single layer of stone of 4.23 cm diameter was placed on a 1/2 slope. The vertical thickness of the stone layer was 4.73 cm in comparison to 14 cm in Fig. 2. The 9-cm width of the 18.5-cm wide crest was impermeable and narrower than the 55-cm wide crest for the OS tests in Fig. 2. The crest height $R_c = (27.3 - d_t)$ cm was between the crest heights for the S and OS tests and the values of T_p and H_{rms} were somewhat smaller as listed in Table 3. The measured reflection coefficients for the revetment with the 1/2 slope were in the range of 0.38 – 0.43 in comparison to the range of 0.19 – 0.23 for the 1/5 permeable slopes. In this revetment experiment, wave runup and fluid velocities were not measured but a wave gauge placed in the middle of the 9-cm wide impermeable crest was used to measure the depth of overtopping water and obtain the probability of wave overtopping as the ratio between the number of overtopping events and the number of incident zero-upcrossing waves. These O tests are used in the following to examine the effect of infiltration on the wave overtopping rate.

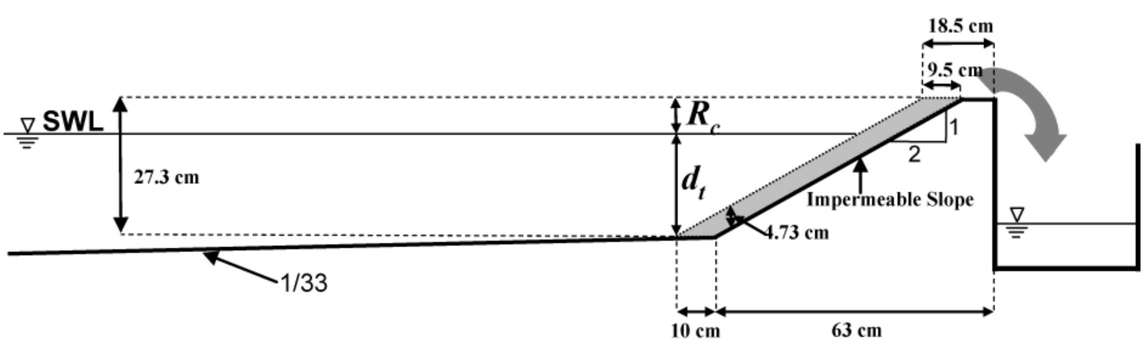

Fig. 3: Overtopping tests for 1/2 slope with single layer of stone.

Table 3: Wave characteristics at wave gauge 1 for overtopping (O) tests.

Test	d_1 [cm]	T_p [s]	H_{rms} [cm]	d_t [cm]	R_c [cm]	q_o [cm^2/s]	r
A11A	26.8	2.5	7.4	14.3	13	1.76	0.41
A12A	26.8	2.0	7.5	14.3	13	1.86	0.41
A21A	26.8	2.5	7.7	14.3	13	1.29	0.41
A22A	26.8	2.0	8.2	14.3	13	1.37	0.38
B12A	27.8	2.0	7.6	15.3	12	2.90	0.41
B22A	27.8	2.0	8.3	15.3	12	2.30	0.39
C11A	28.8	2.5	7.9	16.3	11	4.79	0.41
C12A	28.8	2.0	7.9	16.3	11	4.89	0.42
C21A	28.8	2.5	8.0	16.3	11	3.58	0.43
C22A	28.8	2.0	8.5	16.3	11	4.20	0.39
D12A	29.8	2.0	7.9	17.3	10	7.10	0.43
D22A	29.8	2.0	8.5	17.3	10	5.80	0.40

d_1 =still water depth at wave gauge 1; T_p = spectral peak period; H_{rms} = root-mean-square wave height; d_t = toe depth; R_c = crest height; q_o = overtopping rate; r = reflection coefficient.

2.2 WAVE RUNUP DISTRIBUTION

The runup height R is defined as the crest height above SWL of the temporal variation of the shoreline elevation η_r. The measured time series of $\left[\eta_r(t) - \overline{\eta}_r\right]$ are analyzed using a zero-upcrossing method to identify the crests in the time series. This procedure is the same as that used for the analysis of the wave crests in the time series of $\eta(t)$ except that the wave crest is defined as the height above the mean water level. Tables 4 and 5 show the mean, $\overline{\eta}_r$, and standard deviation, σ_r, of the shoreline elevation η_r above SWL, the significant runup height $R_{1/3}$ and the runup height $R_{2\%}$ corresponding to 2% exceedance probability measured by the runup wire for the seepage (S) and overtopping and seepage (OS) tests. It is noted that the wave setup $\overline{\eta}_r$ of the shoreline was in the range of 0.5 – 3 cm for both experiments and not negligible.

The runup height R above SWL has been fitted to the Rayleigh distribution (e.g., Van der Meer and Janssen 1995) and the Weibull distribution (Van der Meer 1992). The measured distribution of the runup height $\left(R-\overline{\eta}_r\right)$ above the mean level $\overline{\eta}_r$ is fitted to the Weibull distribution

$$P\left(R\right)=\exp\left[-2\left(\frac{R-\overline{\eta}_r}{R_{1/3}-\overline{\eta}_r}\right)^{\kappa}\right] \tag{1}$$

where $P(R)$ = exceedance probability of the runup height R above SWL; $R_{1/3}$ = significant runup height defined as the average of 1/3 highest values of *R*; and κ = shape parameter with κ = 2 for the Rayleigh distribution. Fig. 4 compares the measured exceedance probability with the Rayleigh and Weibull distributions for the 22 S and OS tests where use is made of the measured values of $R_{1/3}$ and $\overline{\eta}_r$ for each test. The Rayleigh distribution with κ = 2 in Eq. (1) yields fair agreement only for the case of no or little wave overtopping. The value of κ for the Weibull distribution for each test is predicted by the following empirical formula:

$$\kappa=2+0.5R_*^{-3} \quad ; \quad R_*=\left(R_c-\overline{\eta}_r\right)/\left(R_{1/3}-\overline{\eta}_r\right) \tag{2}$$

Table 4: Runup statistics and Weibull shape parameter κ for S tests.

TEST	Runup Wire				R_c [cm]	Measured κ	Predicted κ
	$\overline{\eta_r}$ [cm]	σ_r [cm]	$R_{1/3}$ [cm]	$R_{2\%}$ [cm]			
RS20B1	2.01	3.62	10.31	13.31	18.60	2.18	2.06
RS20B2	2.43	3.66	10.71	13.91	18.60	2.05	2.07
RS20C1	0.48	3.66	9.76	13.59	18.60	1.94	2.07
RS20C2	1.26	3.75	10.88	14.03	18.60	2.37	2.09
RS22B1	2.21	4.51	11.44	14.07	16.60	2.68	2.13
RS22B2	2.68	4.24	11.34	14.44	16.60	2.19	2.12
RS22C1	1.41	4.07	11.18	14.60	16.60	2.24	2.13
RS22C2	1.37	4.03	11.18	14.60	16.60	2.25	2.13
RS24B1	2.45	4.83	12.05	14.12	14.60	3.44	2.25
RS24B2	3.15	4.75	12.73	15.66	14.60	2.51	2.29
RS24C1	1.72	4.50	11.62	14.98	14.60	2.30	2.23
RS24C2	1.04	4.62	11.28	14.71	14.60	2.32	2.22

Table 5: Runup statistics and Weibull shape parameter κ for OS tests.

TEST	Runup Wire				R_c [cm]	Measured κ	Predicted κ
	$\overline{\eta_r}$ [cm]	σ_r [cm]	$R_{1/3}$ [cm]	$R_{2\%}$ [cm]			
RO20B1	2.43	3.95	10.77	13.36	9.70	2.48	2.75
RO20C1	1.30	3.74	10.22	12.95	9.70	2.51	2.60
RO22B1	2.21	4.24	10.47	11.87	7.70	4.30	3.70
RO22B2	1.98	4.23	10.28	11.74	7.70	4.13	3.53
RO22C1	1.03	3.90	9.73	11.50	7.70	3.61	3.11
RO22C2	0.88	3.94	9.76	11.88	7.70	3.13	3.10
RO24B1	0.70	4.12	8.89	10.04	5.70	5.12	4.20
RO24B2	1.15	4.29	9.59	10.82	5.70	4.90	5.18
RO24C1	0.84	3.85	8.83	10.26	5.70	4.06	4.22
RO24C2	0.94	3.98	9.02	10.33	5.70	4.47	4.44

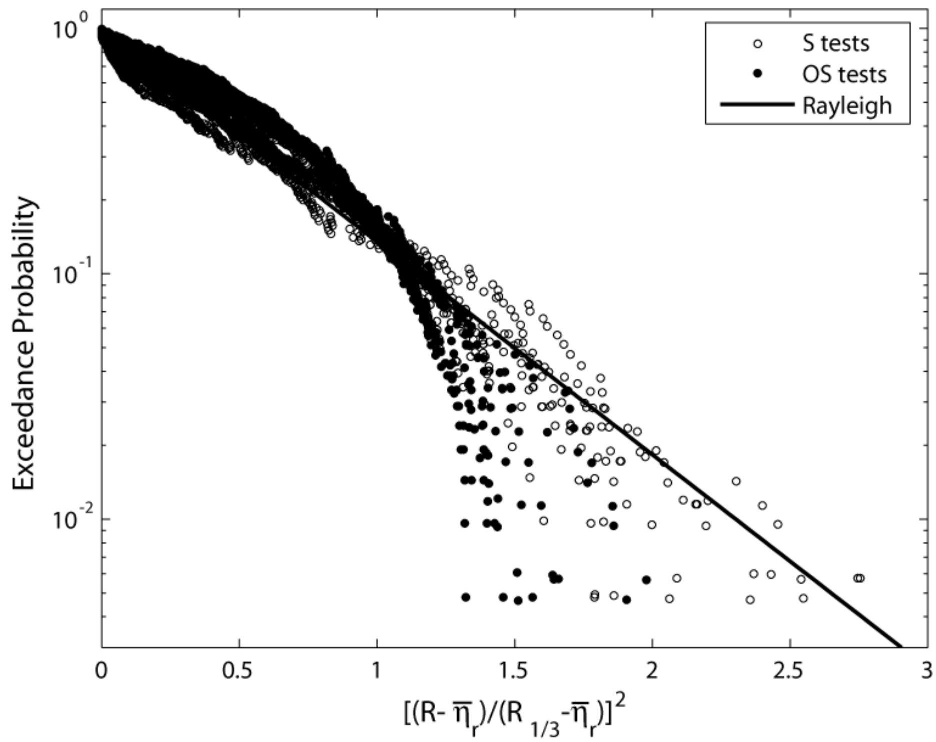

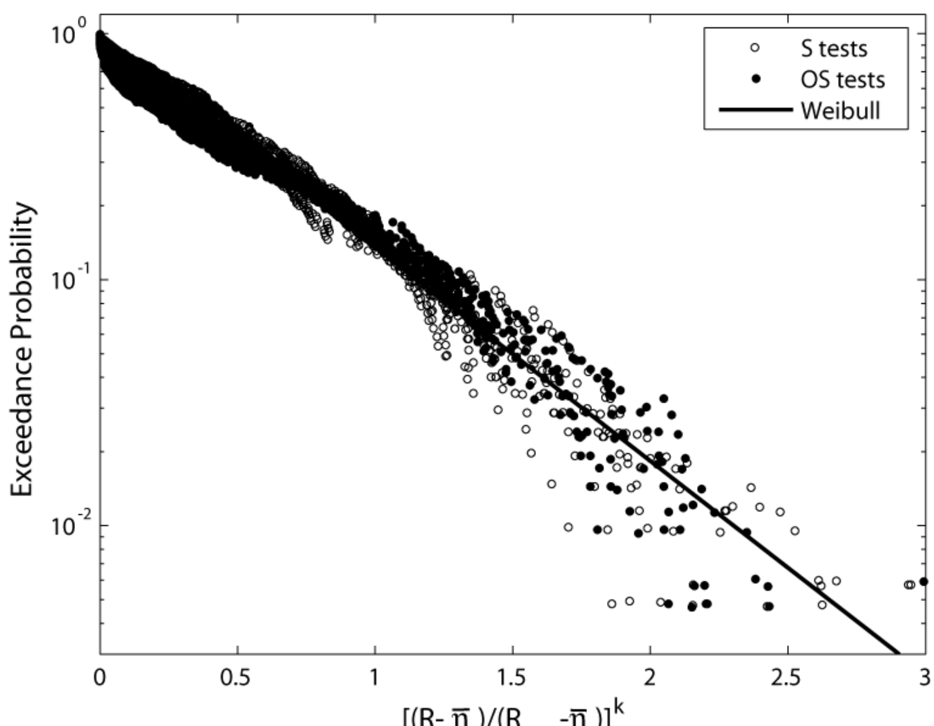

Fig. 4: Comparisons of measured exceedance probability distributions of runup height *R* with Rayleigh (top) and Weibull (bottom) distributions.

Fig. 5 compares the empirical formula for κ with the measured values of the shape parameter for the S and OS tests. The measured and predicted values of κ are listed in Tables 4 and 5 where the measured κ has been calculated from the measured values of $R_{2\%}$, $R_{1/3}$ and $\overline{\eta}_r$ for each test using the following expression based on Eq. (1):

$$P\left(R_{2\%}\right)=\exp\left[-2\left(\frac{R_{2\%}-\overline{\eta}_r}{R_{1/3}-\overline{\eta}_r}\right)^{\kappa}\right]=0.02 \quad \Rightarrow \quad \kappa=\frac{\ln\left[-0.5\ln\left(0.02\right)\right]}{\ln\left[\left(R_{2\%}-\overline{\eta}_r\right)/\left(R_{1/3}-\overline{\eta}_r\right)\right]} \qquad (3)$$

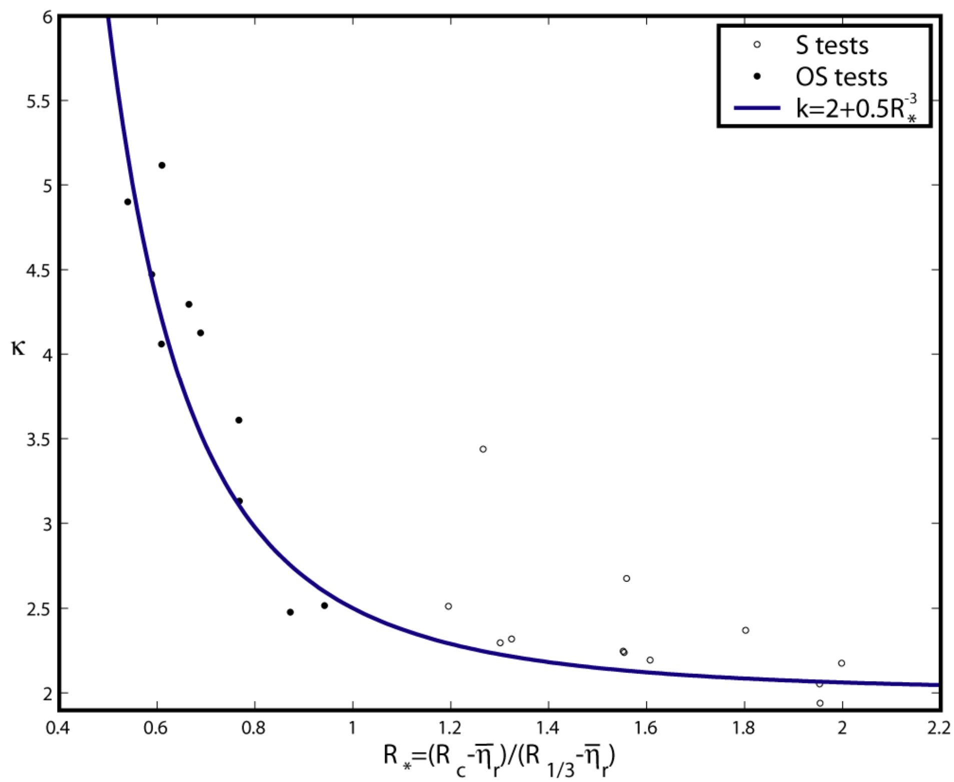

Fig. 5: Comparison of the measured shape parameter κ for the Weibull distribution and the empirical formula $\kappa = 2+0.5R_*^{-3}$ for S and OS tests.

Fig. 6 shows the comparison between the measured normalized $R_{2\%}$ expressed as $\left(R_{2\%}-\overline{\eta}_r\right)/\left(R_{1/3}-\overline{\eta}_r\right)$ and the predicted relationship using Eqs. (2) and (3) as a function of the normalized crest height R_*. The figure shows the decrease of the normalized $R_{2\%}$ due to the decrease of the normalized crest height R_*.

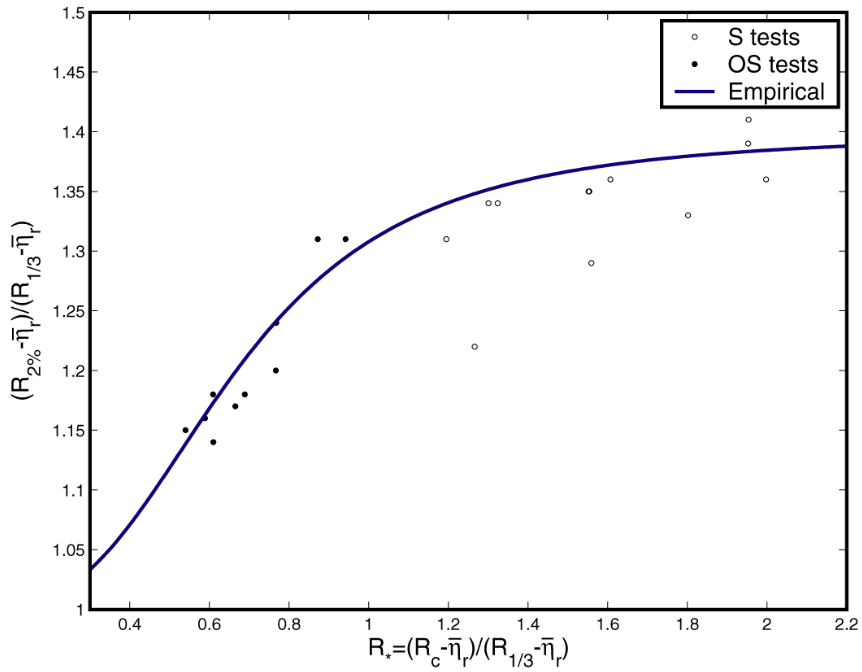

Fig. 6: Comparison of the measured and empirical normalized $R_{2\%}$ vs. the normalized crest height R_* for S and OS tests.

The normalized crest height R_* is related to the probability P_o of R exceeding R_c in Eq. (1)

$$P_o = \exp\left(-2R_*^{\kappa}\right) \tag{4}$$

which may be regarded as the wave overtopping probability because the runup wire height δ_r = 2 cm was about a half of the nominal stone diameter D_{n50} = 3.4 cm and relatively small. The Weibull distribution with κ given by Eq. (2) yields fair agreement for both the S and OS tests because it accounts for the increase of κ with the decrease of R_*.

Fig. 7 shows the wave overtopping probability P_o as a function of the normalized crest height R_* for the Rayleigh distribution with $\kappa = 2$ and the Weibull distribution with κ given by Eq. (2). The difference between the two distributions becomes large for P_o exceeding about 0.3. This explains the use of the Rayleigh distribution for designing the crest height of a coastal structure for minor overtopping. For the case of major overtopping, the Rayleigh distribution underpredicts the wave overtopping probability P_o for given R_*.

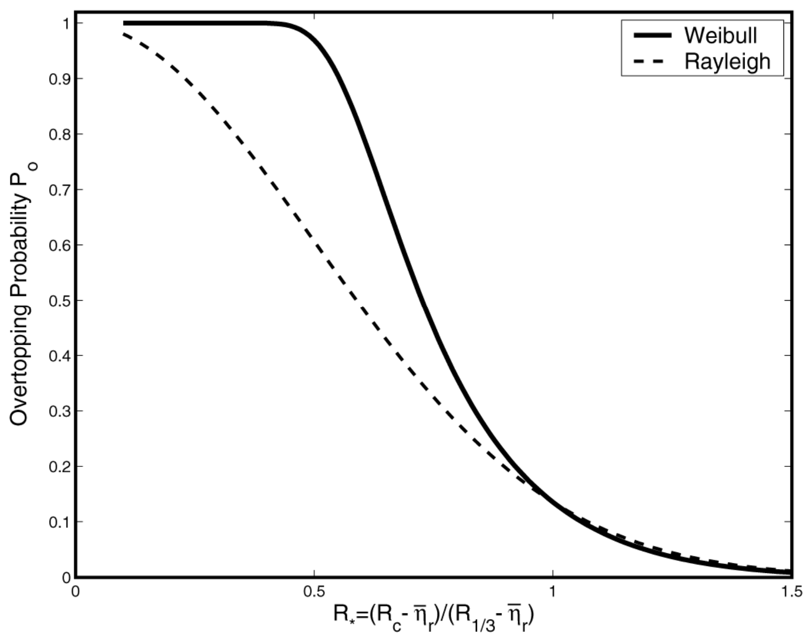

Fig. 7: Overtopping probability as a function of normalized crest height for Rayleigh and Weibull distributions.

The use of Eqs. (2) and (4) requires the prediction of $\overline{\eta_r}$ and $R_{1/3}$. It will be shown later that the numerical model is able to predict $\overline{\eta_r}$ and σ_r. Kobayashi et al. (2006a) used the following formula for the significant runup height $R_{1/3}$

$$R_{1/3} = \overline{\eta_r} + \left(2 + \tan\theta\right)\sigma_r \tag{5}$$

where θ = slope angle from the horizontal at the still water shoreline. For the S and OS tests, $\tan\theta = 1/5$ as shown in Fig. 2, whereas $\tan\theta = 1/2$ for the O tests in Fig. 3. For the Gaussian distribution of the runup elevation η_r, $\left(R_{1/3} - \overline{\eta_r}\right) = 2\sigma_r$. Fig. 8 compares the probability density functions of the measured normalized shoreline elevation $\eta_* = \left(\eta_r - \overline{\eta_r}\right)/\sigma_r$ with the Gaussian distribution given by $f\left(\eta_*\right) = \left(1/\sqrt{2\pi}\right)\exp\left(-0.5\eta_*^2\right)$. The Gaussian distribution turns out to be a reasonable first approximation for both S and OS tests, especially for $\eta_* > 1.5$. Kobayashi et al. (2006a) added the slope adjustment term in Eq. (5) to improve the agreement for $R_{1/3}$ for 57 runup tests with $\tan\theta = 1/5$ and 1/2 in the absence of seepage and overtopping. Eq. (5) turns out to be satisfactory for the present S and OS tests as will be shown later.

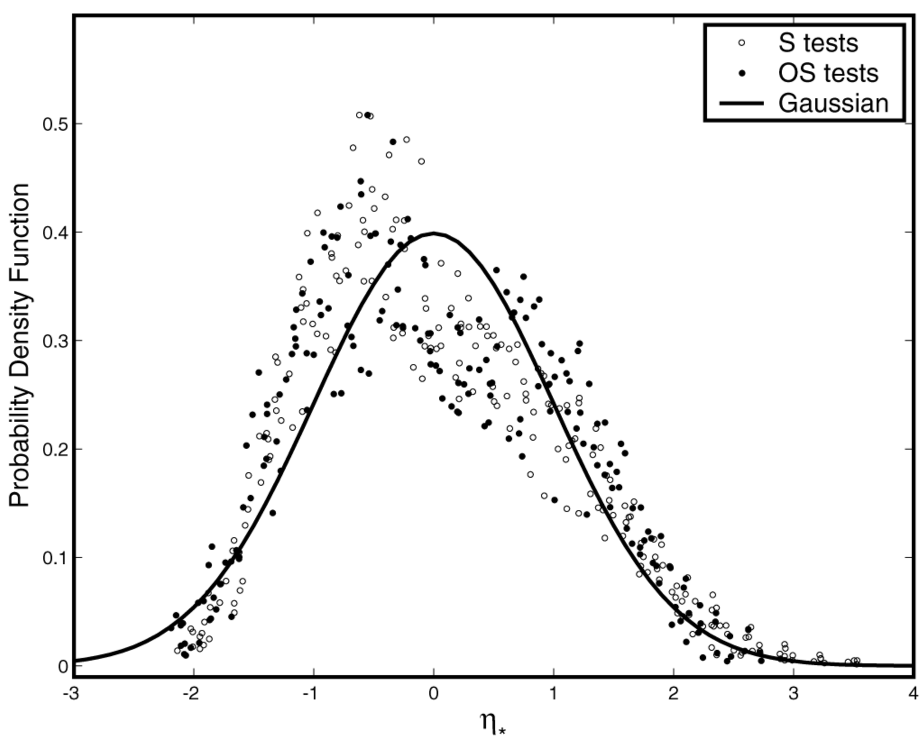

Fig. 8: Comparison of the Gaussian and measured probability density functions of the normalized runup elevation $\eta_* = \left(\eta_r - \overline{\eta_r}\right)/\sigma_r$ for all S and OS tests.

CHAPTER 3 NUMERICAL MODEL

The numerical wave model based on the time-averaged continuity, momentum and energy equations developed by Kobayashi et al. (2006b) is presented first in this chapter. The governing equations and simplifications are briefly reviewed. The numerical model is further extended to account for wave seepage through a permeable layer and overtopping by adding the resulting landward mass flux in the continuity equation. Second, semi-empirical seepage and overtopping models are developed using the computed variables on the permeable slope and accounting for infiltration effects on the permeable crest.

3.1 TIME-AVERAGED WAVE PROPAGATION MODEL

The numerical model based on the time-averaged continuity, momentum and energy equations developed by Kobayashi et al. (2006b) is extended here to allow the landward water flux due to seepage and overtopping. In this numerical model, the cross-shore coordinate x is positive onshore. The vertical coordinate z is positive upward with $z = 0$ at SWL. The upper and lower boundaries of the permeable stone layer are located at $z = z_b$ and z_p, respectively, where the lower boundary is assumed to be impermeable, as depicted in Fig. 9. The beach in front of the permeable slope is assumed to be impermeable and $z_b = z_p$ on the beach and the impermeable crest of the revetment for the O tests. The instantaneous water depth and free surface elevation are denoted by h and η, respectively, and $h = (\eta - z_b)$. The horizontal fluid velocity is represented by the depth-averaged velocity *u*.

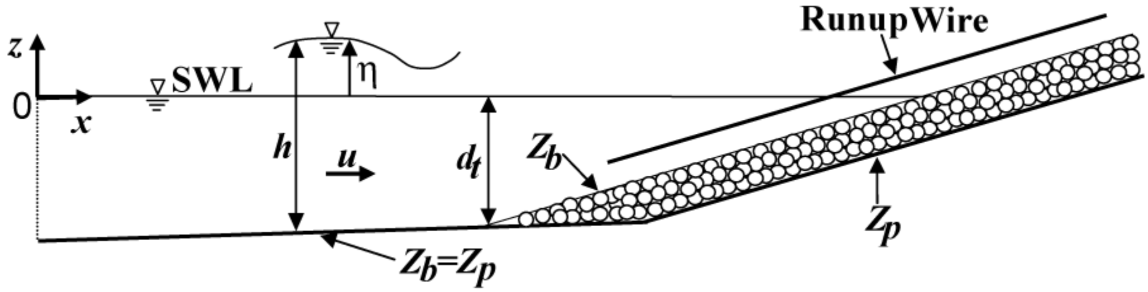

Fig. 9: Definition sketch for time-averaged wave propagation model on permeable slope.

The time-averaged momentum and energy equations are expressed as

$$\frac{dS_{xx}}{dx} = -\rho g \bar{h} \frac{d\bar{\eta}}{dx} - \tau_b \quad ; \quad \frac{dF}{dx} = -D_B - D_f - D_r \tag{6}$$

where S_{xx} = cross-shore radiation stress; ρ = fluid density; g = gravitational acceleration; $\bar{h}$ = mean water depth with the overbar denoting time averaging; $\bar{\eta}$ = wave setup or setdown; τ_b = time-averaged bottom shear stress; and D_B, D_f and D_r = time-averaged energy dissipation rate per unit horizontal area due to wave breaking, bottom friction, and porous flow resistance, respectively. Linear wave theory for onshore progressive waves is used to estimate S_{xx} and F

$$S_{xx} = \rho g \sigma_\eta^2 (2n - 0.5) \quad ; \quad F = \rho g C_g \sigma_\eta^2 \tag{7}$$

where σ_η = standard deviation of η; and $n = C_g / C_p$ with C_g and C_p = group velocity and phase velocity in the mean water depth $\bar{h}$ corresponding to the spectral peak period T_p of incident waves.

The bottom shear stress τ_b and the corresponding dissipation rate D_f are expressed using the formulas based on the quadratic drag force based on the horizontal velocity u. The mean and standard deviation of u are denoted by $\bar{u}$ and σ_u, respectively. The Gaussian distribution of u and the equivalency of the time and probabilistic averaging are assumed to express τ_b and D_f in terms of $\bar{u}$ and σ_u

$$\tau_b = \frac{1}{2}\rho f_b \sigma_u^2 G_2(u_*) \quad ; \quad D_f = \frac{1}{2}\rho f_b \sigma_u^3 G_3(u_*) \quad ; \quad u_* = \frac{\bar{u}}{\sigma_u} \tag{8}$$

where f_b = bottom friction factor which is taken as $f_b = 0$ in the area of $z_b = z_p$ and $f_b = 0.01$ in the area covered with the stone (Kobayashi et al. 2006b). The analytical functions $G_2(r)$ and $G_3(r)$ for the arbitrary variable r are given by Kobayashi et al. (2005) and can be approximated as $G_2 \simeq 1.64\, r$ and $G_3 \simeq (1.6 + 2.6\, r^2)$ for $|r| < 1$. The energy dissipation rate D_B due to wave breaking is estimated using the formula by Battjes and Stive (1985) which is modified to increase D_B on a steep slope in very shallow water (Kobayashi et al. 2005, 2006b).

The standard deviation σ_u is estimated using the relationship between σ_u and σ_η based on linear shallow-water wave theory

$$\sigma_u = \sigma_* \left(g\bar{h}\right)^{0.5} \quad ; \quad \sigma_* = \sigma_\eta / \bar{h} \tag{9}$$

The mean $\bar{u}$ is estimated using the time-averaged, vertically-integrated continuity equation

$$\sigma_u \sigma_\eta + \bar{u}\,\bar{h} + \bar{v}\,h_p = q_{os} \qquad ; \qquad q_{os} = q_o + q_s \tag{10}$$

where $\sigma_u \sigma_\eta$ = wave-induced onshore flux; $\bar{u}\,\bar{h}$ = water flux due to the mean current $\bar{u}$; $\bar{v}\,h_p$ = water flux inside the permeable layer of the vertical height h_p = $(z_b - z_p)$ due to the time-averaged horizontal discharge velocity $\bar{v}$; q_{os} = combined overtopping and seepage rate; q_o = wave overtopping rate; and q_s = seepage rate. Substitution of Eq. (9) into Eq. (10) yields

$$\bar{u} = -\sigma_*^2 \left(g\bar{h} \right)^{0.5} + \frac{q_{os} - \bar{v}h_p}{\bar{h}} \tag{11}$$

The energy dissipation rate D_r in Eq. (6) is estimated using the discharge velocity v whose probability distribution is assumed to be Gaussian

$$D_r = \rho h_p \left[\alpha \sigma_v^2 \left(1 + v_*^2 \right) + \beta \sigma_v^3 G_3 \left(v_* \right) \right] \qquad ; \qquad v_* = \frac{\bar{v}}{\sigma_v} \tag{12}$$

where σ_v = standard deviation of v; G_3 = same function as in Eq. (8) except for $r = v_*$; and α and β = laminar and turbulent flow resistance coefficients. Kobayashi et al. (2006b) modified the formulas of α and β by van Gent (1995) for irregular waves in the form

$$\alpha = \alpha_o \left(\frac{1 - n_p}{n_p} \right)^2 \frac{\nu}{D_{n50}^2} \; ; \beta = \left(\beta_1 + \frac{\beta_2}{\sigma_v} \right); \beta_1 = \frac{\beta_o \left(1 - n_p \right)}{n_p^3 D_{n50}} \; ; \beta_2 = \frac{7.5 \beta_o \left(1 - n_p \right)}{\sqrt{2} n_p^2 T_p} \tag{13}$$

where α_o and β_o = empirical parameters calibrated as α_o = 1,000 and β_o = 5; n_p = porosity of the stone; D_{n50} = nominal stone diameter; ν = kinematic viscosity of water $\left(\nu \simeq 0.01 \text{cm}^2/\text{s} \right)$; and T_p = spectral peak period. The mean $\bar{v}$ and standard deviation σ_v are estimated assuming the local force balance between the horizontal gradient of hydrostatic pressure and the flow resistance inside the permeable layer

$$\left(\alpha + 1.64\beta\sigma_v\right)\bar{v} = -g\frac{d\bar{\eta}}{dx} \quad ; \quad \alpha\sigma_v + 1.9\beta\sigma_v^2 = gk_p\bar{h}\sigma_* \tag{14}$$

where k_p = linear wave number based on $\bar{h}$ and T_p. Eq. (14) can be solved analytically to obtain σ_v and $\bar{v}$ for known $k_p\bar{h}\sigma_*$ and $d\bar{\eta}/dx$.

Eqs. (6) - (14) are the same as those used by Kobayashi et al. (2006a, b) except for the combined overtopping and seepage rate $q_{os} = 0$ in their computations. The empirical parameters in the model are not recalibrated except for the O tests as explained later. The bottom elevation $z_b(x)$ and the impermeable boundary $z_p(x)$ are specified as input. The stone is characterized by its nominal diameter D_{n50} and porosity n_p. The measured values of T_p, $\bar{\eta}$ and $H_{\mathrm{rms}} = \sqrt{8}\,\sigma_\eta$ at wave gauge 1 are specified at the seaward boundary $x = 0$ outside the surf zone. The landward-marching computation of $\bar{\eta}$, σ_η, $\bar{u}$, σ_u, $\bar{v}$ and σ_v is continued until the computed value of $\bar{h} = \left(\bar{\eta} - z_b\right)$ or σ_η becomes negative in the region of $\bar{h}$ on the order of 0.1 cm. Since the formulas for q_{os} presented in the next section require the computed quantities on the permeable slope, this landward computation starting from q_{os} = 0 is repeated until the assumed and computed values of q_{os} converge within the measurement uncertainty of 0.1 cm^2/s. This convergency is normally obtained after several iterations.

The time-averaged model based on Eqs. (6) - (14) neglects reflected waves. The onshore energy flux F in Eq. (6) decreases landward due to wave breaking, bottom friction and porous flow resistance. The residual energy flux F_{SWL} at the still water shoreline located at $z_b = 0$ is assumed to be reflected and propagate seaward. Kobayashi et al. (2005, 2006a) crudely estimated the root-mean-square wave height $(H_{\mathrm{rms}})_r$ due to the reflected wave energy flux using linear wave theory

$$(H_{rms})_r = \left[8F_{SWL}/\left(\rho g C_g\right)\right]^{0.5} \tag{15}$$

where the group velocity C_g is assumed to be the same for the incident and reflected waves.

3.2 SEEPAGE AND OVERTOPPING MODEL

Kobayashi et al. (2006a) developed a probabilistic model for irregular wave runup using the computed $\bar{\eta}(x)$ and $\sigma_\eta(x)$ on the permeable slope. A runup wire was used to measure the shoreline oscillations above the slope as shown in Fig. 10. The vertical height δ_r of the wire above the average stone surface was 2 cm. The wire measures the instantaneous elevation $\eta_r(t)$ above SWL of the intersection between the wire and the free surface unlike the wave gauge that measured $\eta(t)$ at given x. Fig. 10 depicts an intuitive method used to estimate the mean $\bar{\eta}_r$ and standard deviation σ_r of $\eta_r(t)$. The probabilities of η exceeding $\left(\bar{\eta}+\sigma_\eta\right)$, $\bar{\eta}$ and $\left(\bar{\eta}-\sigma_\eta\right)$ are assumed to be the same as the probabilities of η_r exceeding $\left(\bar{\eta}_r+\sigma_r\right)$, $\bar{\eta}_r$ and $\left(\bar{\eta}_r-\sigma_r\right)$, respectively. The elevations of Z_1, Z_2 and Z_3 of the intersections of $\left(\bar{\eta}+\sigma_\eta\right)$, $\bar{\eta}$ and $\left(\bar{\eta}-\sigma_\eta\right)$ with the runup wire are obtained using the computed $\bar{\eta}(x)$ and $\sigma_\eta(x)$ together with the wire elevation $\left[z_b(x)+\delta_r\right]$. The obtained elevations are assumed to correspond to $Z_1=\left(\overline{\eta_r}+\sigma_r\right)$, $Z_2=\overline{\eta_r}$ and $Z_3=\left(\bar{\eta}_r-\sigma_r\right)$. The mean and standard deviation of $\eta_r(t)$ are estimated as

$$\overline{\eta_r} = \left(Z_1+Z_2+Z_3\right)/3 \quad ; \quad \sigma_r = \left(Z_1-Z_3\right)/2 \tag{16}$$

where the use of Z_1, Z_2 and Z_3 to estimate $\overline{\eta}_r$ is slightly more reliable than $\overline{\eta}_r = Z_2$ because of the sensitivity of $\overline{\eta_r}$ to the wire height δ_r.

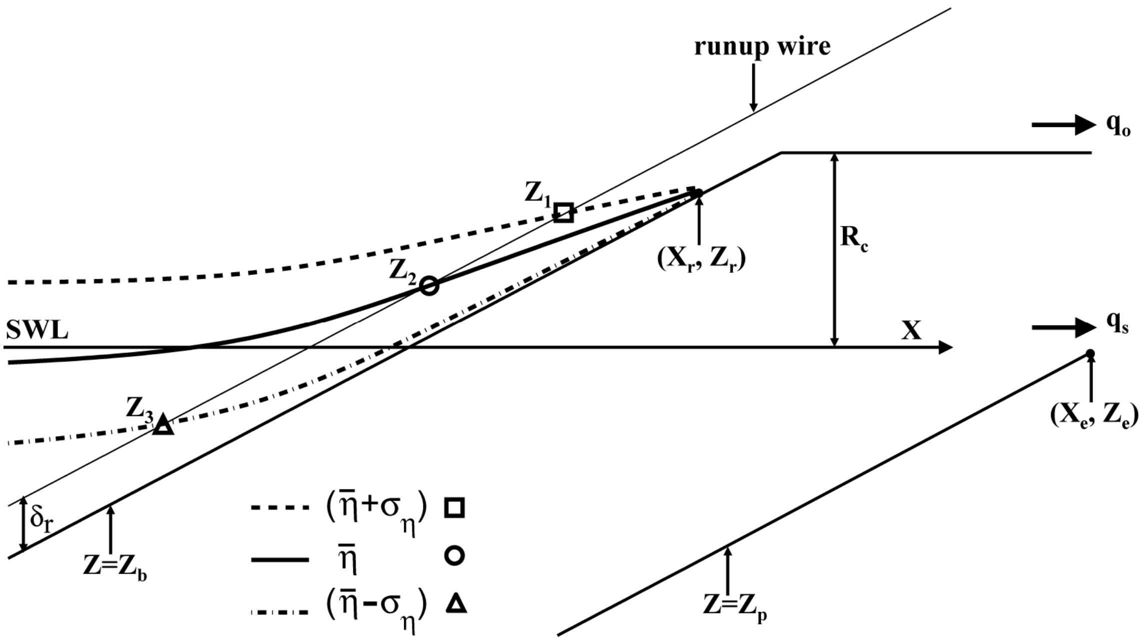

Fig. 10: Definition sketch for overtopping and seepage model.

Available empirical formulas for the wave overtopping rate q_o express q_o in terms of wave parameters at the toe of the slope, slope characteristics and the structure crest height R_c (e.g. Van der Meer and Jansen 1995). The present numerical model allows one to develop a formula for q_o using the computed variables on the permeable slope. The overtopping rate q_o is expressed empirically as

$$q_o / q_{SWL} = a\left(P_o\right)^b \qquad ; \qquad q_{SWL} = \sigma_\eta \sigma_u \;\text{ at }\; x = x_{SWL} \tag{17}$$

where q_{SWL} = wave-induced onshore flux $\sigma_\eta\sigma_u$ in the continuity equation (10) evaluated at the still water shoreline SWL located at $x = x_{SWL}$; a and b = empirical parameters. Eq. (17) is based on the assumption that q_o is of the order of q_{SWL} if $P_o = 1$ and no infiltration occurs.

The wave overtopping probability P_o is given by Eq. (4) and depends on the normalized crest height R_*.

The parameters a and b are assumed to depend on the horizontal width L_p of the permeable surface above the upper limit of wave setup located at (x_r, z_r) in Fig. 10 where this point is the end of the landward-marching computation using Eqs. (6) - (14). The use of the horizontal distance L_p may be reasonable for vertical infiltration. For the S and OS tests in Fig. 2, $L_p = (x_e - x_r)$ where x_e = cross-shore location of the edge of the overtopping tank. For the O tests in Fig. 3, L_p is the horizontal distance between x_r and the landward edge of the permeable layer where z_b becomes equal to z_p at the distance of 9 cm from the tank edge. For the data sets listed in Table 1 – 3, the empirical parameters a and b can be expressed as

$$a = \exp\left(-0.1 L_*\right) \quad ; \quad b = 1 + 0.1 L_* \quad ; \quad L_* = L_p / D_{n50} \tag{18}$$

where L_* = infiltration width normalized by the nominal stone diameter D_{n50}. The value of L_* crudely represents the horizontal number of stones above the maximum wave setup. For $L_* = 0$, $a = 1$ and $b = 1$ and Eq. (17) yields $q_o = P_o\ q_{SWL}$. As L_* is increased, a decreases and b increases, resulting in the decrease of q_o / q_{SWL}.

Fig. 11 shows the normalized overtopping rate q_o / q_{SWL} as a function of the normalized crest height R_* for L_* = 2, 5, 10 and 20. The range of L_* is 4.0 – 5.7 and 12.4 – 21.2 for the O and OS tests, respectively. The overtopping rate is sensitive to the normalized infiltration width especially for the case of $R_* > 1$ and $P_o < 0.14$ in view of Fig. 7 and Fig. 11. The empirical formulas for a and b given by Eq. (18) need to be verified using other data sets but Fig. 11 clearly shows the need to account for infiltration for the prediction of the wave overtopping rate q_o.

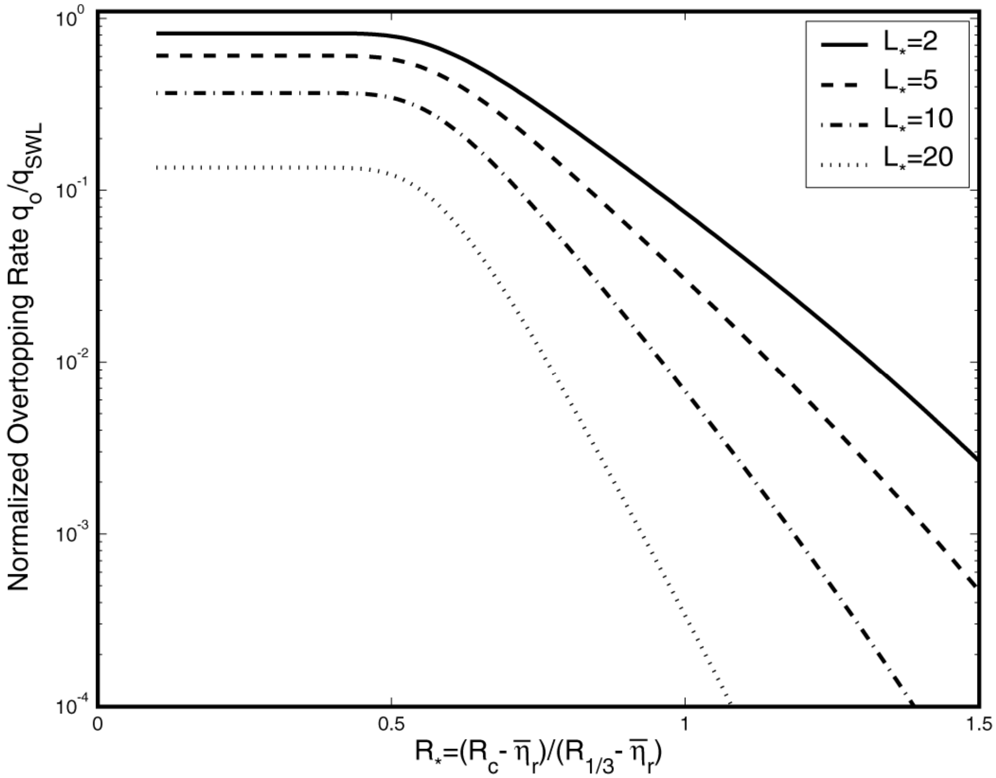

Fig. 11: Normalized overtopping rate as a function of normalized crest height for normalized infiltration width $L_* = 2, 5, 10$ and 20.

On the other hand, the seepage flow in the permeable layer is assumed to be horizontal and driven by the wave setup on the seaward slope. In reality, the seepage flow is affected by infiltration and very complex but a simple analysis is performed to obtain a formula for the seepage rate q_s in Eq. (10). The time-averaged cross-shore momentum equation for the horizontal seepage flow may be simplified as

$$\beta_1 v_s^2 + \alpha v_s = g \frac{z_r - z_e}{x_e - x_r} = E \tag{19}$$

where β_1 and α = turbulent and laminar flow resistance coefficients given in Eq. (13) for unidirectional flow for which $\beta_2 = 0$; v_s = time-averaged seepage velocity; and x_e and z_e = cross-shore location and elevation of the landward end of the impermeable surface $z_p(x)$ at the tank edge as shown in Fig. 10. The landward pressure gradient driving the seepage flow is approximated by ρE. Eq. (19) can be solved analytically to obtain the equation of v_s which is simplified as $v_s = \left(E/\beta_1\right)^{0.5}$ for $\alpha^2 \ll \left(4E\beta_1\right)$ where this condition is satisfied for the S and OS tests with α = 0.9 s^{-1} and β_1 = 5.9 cm^{-1}. The seepage rate q_s is assumed to be proportional to $v_s(z_r - z_e)$ and expressed as

$$q_s = 0.2\left(z_r - z_e\right)^{1.5}\left[\frac{g}{\left(x_e - x_r\right)\beta_1}\right]^{0.5} \quad \text{for} \quad z_r > z_e \tag{20}$$

where the coefficient 0.2 is the value calibrated for the S tests and q_s = 0 if $z_r < z_e$. If the landward-marching computation reaches the tank edge, $x_r = x_e$ and $q_s = \overline{v}h_p$ at $x = x_e$ where the water flux $\overline{v}h_p$ in the permeable layer is included in the continuity equation (10).

CHAPTER 4 COMPARISONS WITH EXPERIMENTS

Comparisons of the numerical model with the experiments are shown in this chapter. First, the measured and predicted cross-shore variations of $\bar{\eta}$, σ_η , $\bar{u}$ and σ_u for the 12 seepage (S) tests and 10 overtopping and seepage (OS) tests for the 1/5 permeable slope are presented. Second, the measured wave runup statistics as well as the measured seepage and combine overtopping and seepage rates are compared with the present model and the empirical formulas of Van der Meer and Janssen (1995). Third, for the 1/2 slope overtopping (O) tests, the sensitivity of the results to the breaker ratio parameter γ and the runup wire height δ_r is examined. Last, the effect of the porous layer is discussed and the predicted and measured reflection coefficients for all the tests are compared.

4.1 CROSS-SHORE WAVE TRANSFORMATION

Fig. 12 – Fig. 33 compare the measured and predicted cross-shore variations of the mean and standard deviation of the free surface elevation η and the cross-shore velocity u for

each of the 12 S and 10 OS tests where unreliable velocity data points are not plotted. The dashed and solid lines in these figures correspond to the computed variations with $q_{os} = 0$ for the first landward-marching computation and the converged rate of q_{os} for the last computation, respectively.

The comparisons indicate that the wave setup $\overline{\eta}$ and the standard deviations σ_η and σ_u are affected little by wave seepage and overtopping. For tests RO24B1, RO24B2, RO24C1 and RO24C2, where the crest height $R_c = 5.7$ cm is the smallest, the first computation with $q_{os} = 0$ reaches the landward end located at $x = x_e$ as shown in the last panel of the corresponding figure (Fig. 30 – Fig. 33) which shows $z_b(x)$ and $z_p(x)$. The mean cross-shore velocity $\overline{u}$ computed using Eq. (11) is affected directly by q_{os} and increases with the increase of q_{os} especially above SWL. The numerical model predicts the cross-shore variations of $\overline{\eta}$, σ_η, $\overline{u}$ and σ_u fairly well as has been shown in the previous comparisons by Kobayashi et al. (2005; 2006a, b).

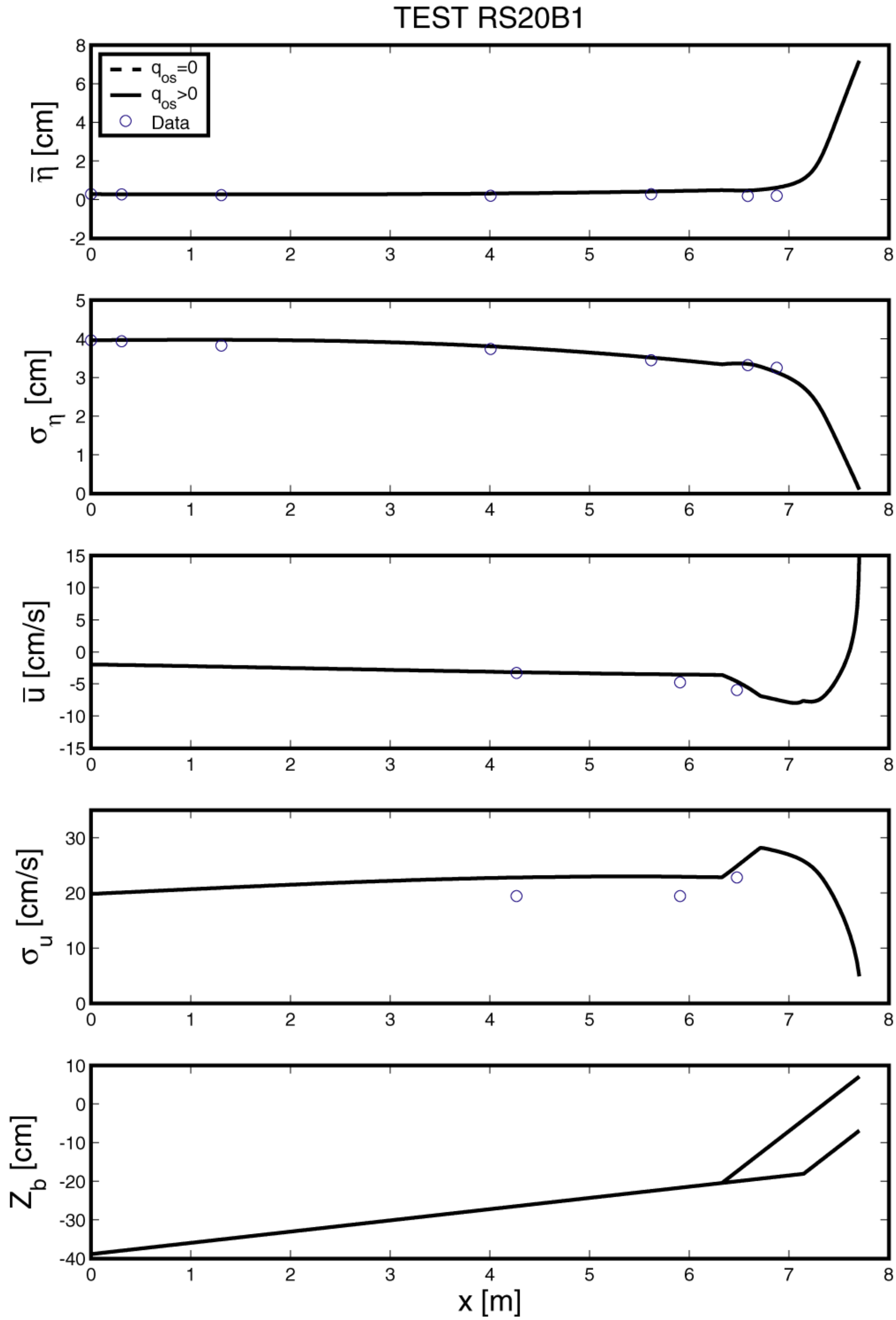

Fig. 12: Measured and predicted cross-shore variations of mean and standard variation of η and u above bottom profile z_b without ($q_{os} = 0$) and with ($q_{os} > 0$) combined overtopping and seepage rate for test RS20B1.

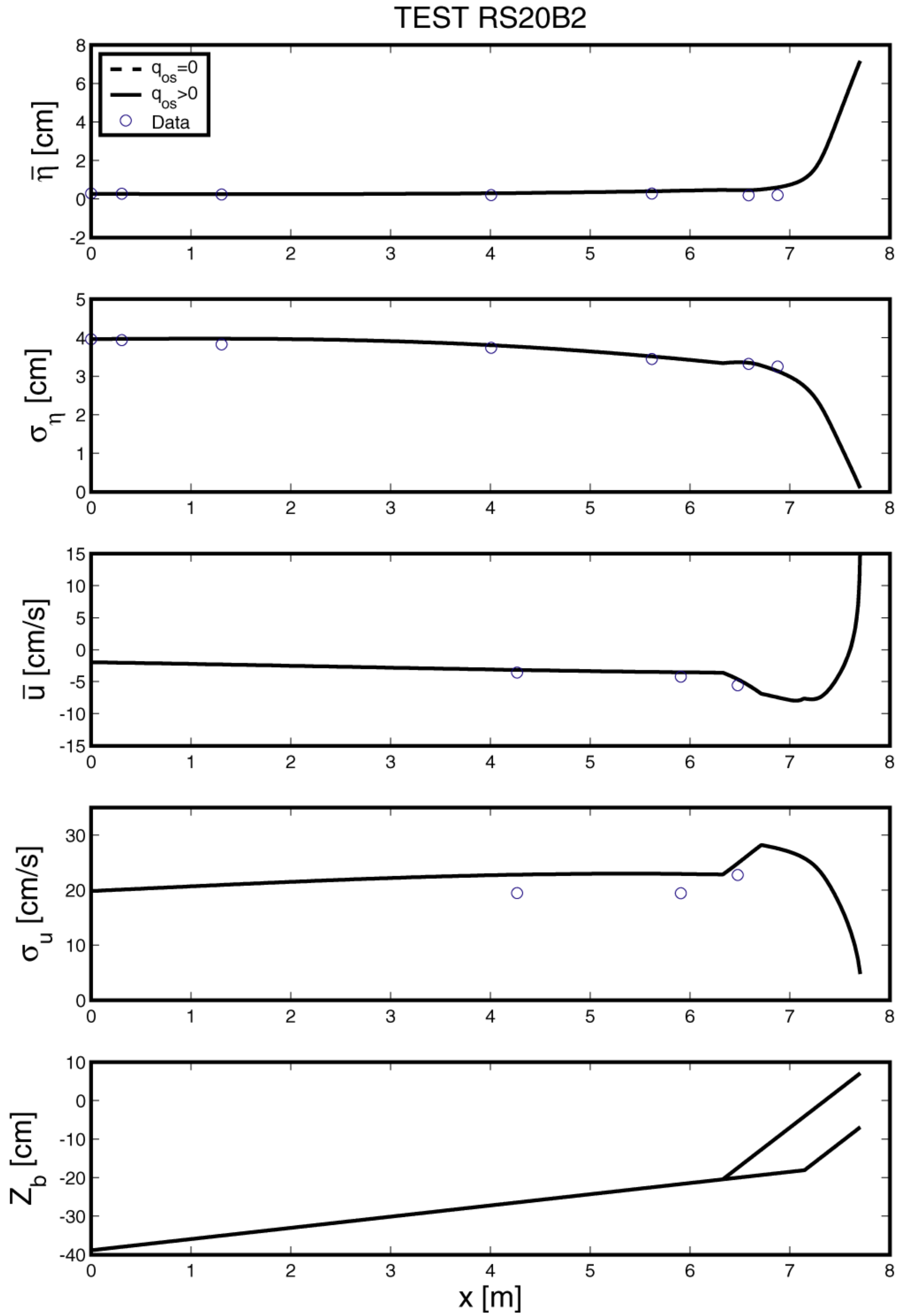

Fig. 13: Measured and predicted cross-shore variations of mean and standard variation of η and u above bottom profile z_b without ($q_{os} = 0$) and with ($q_{os} > 0$) combined overtopping and seepage rate for test RS20B2.

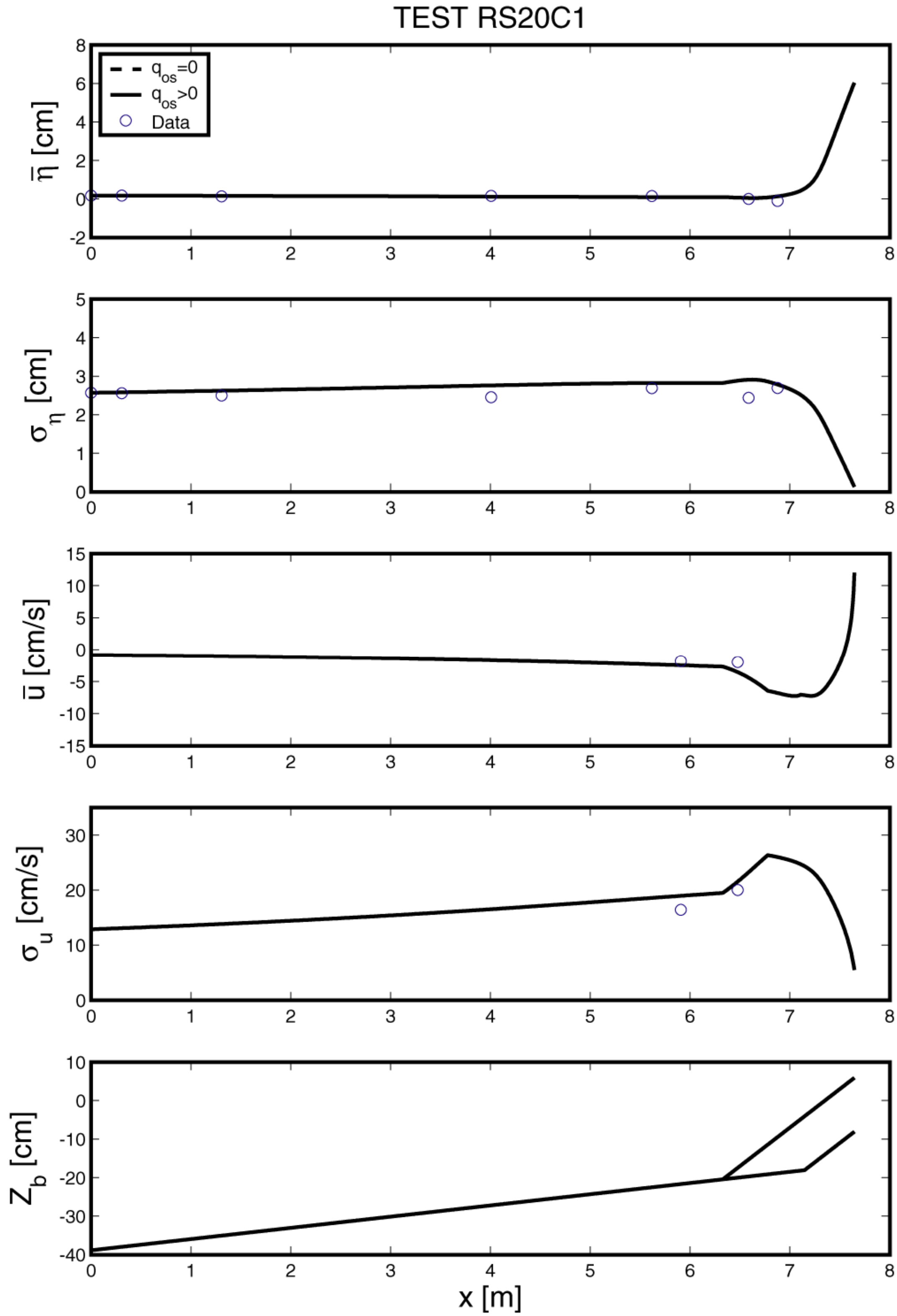

Fig. 14: Measured and predicted cross-shore variations of mean and standard variation of η and u above bottom profile z_b without ($q_{os} = 0$) and with ($q_{os} > 0$) combined overtopping and seepage rate for test RS20C1.

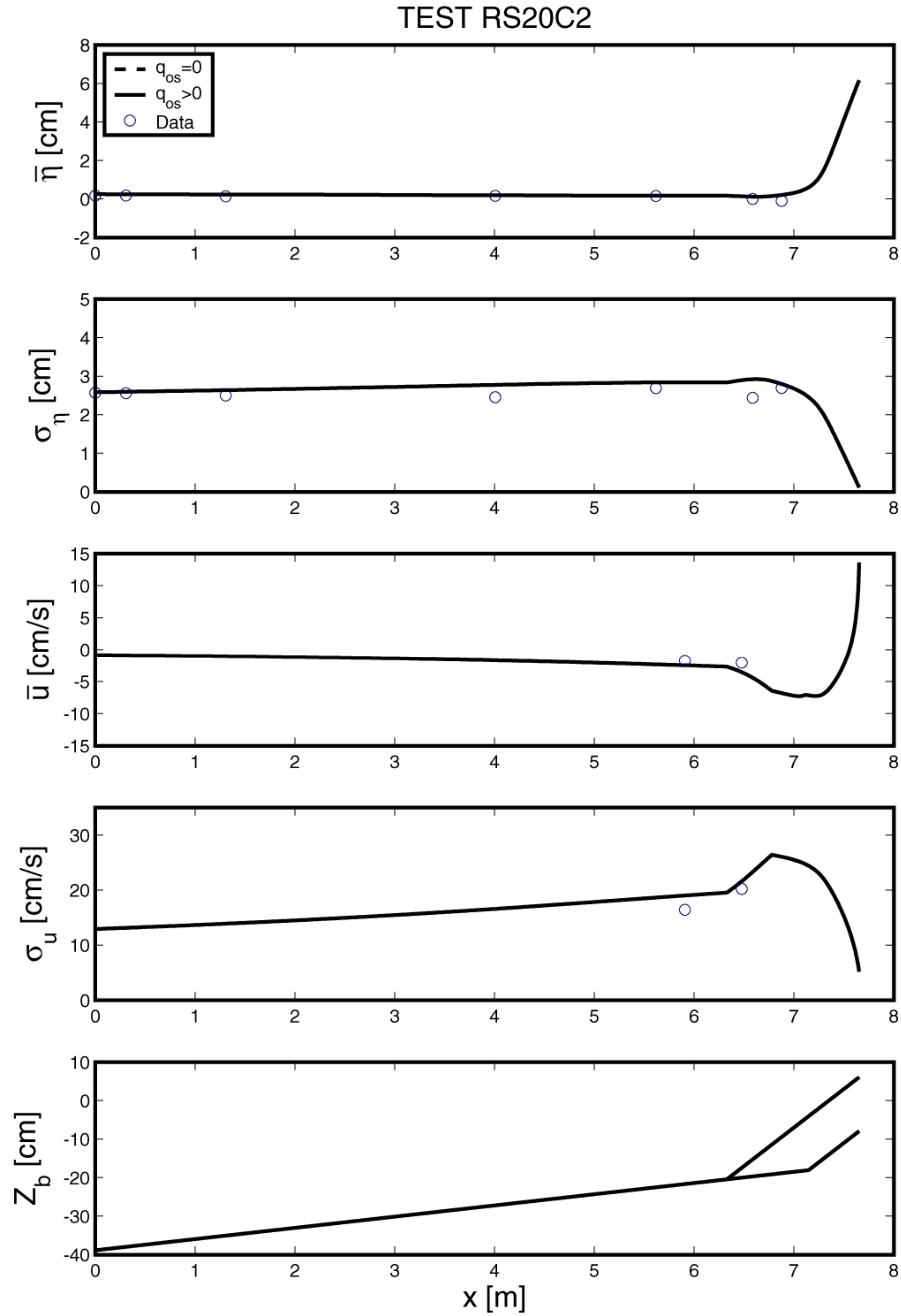

Fig. 15: Measured and predicted cross-shore variations of mean and standard variation of η and u above bottom profile z_b without ($q_{os} = 0$) and with ($q_{os} > 0$) combined overtopping and seepage rate for test RS20C2.

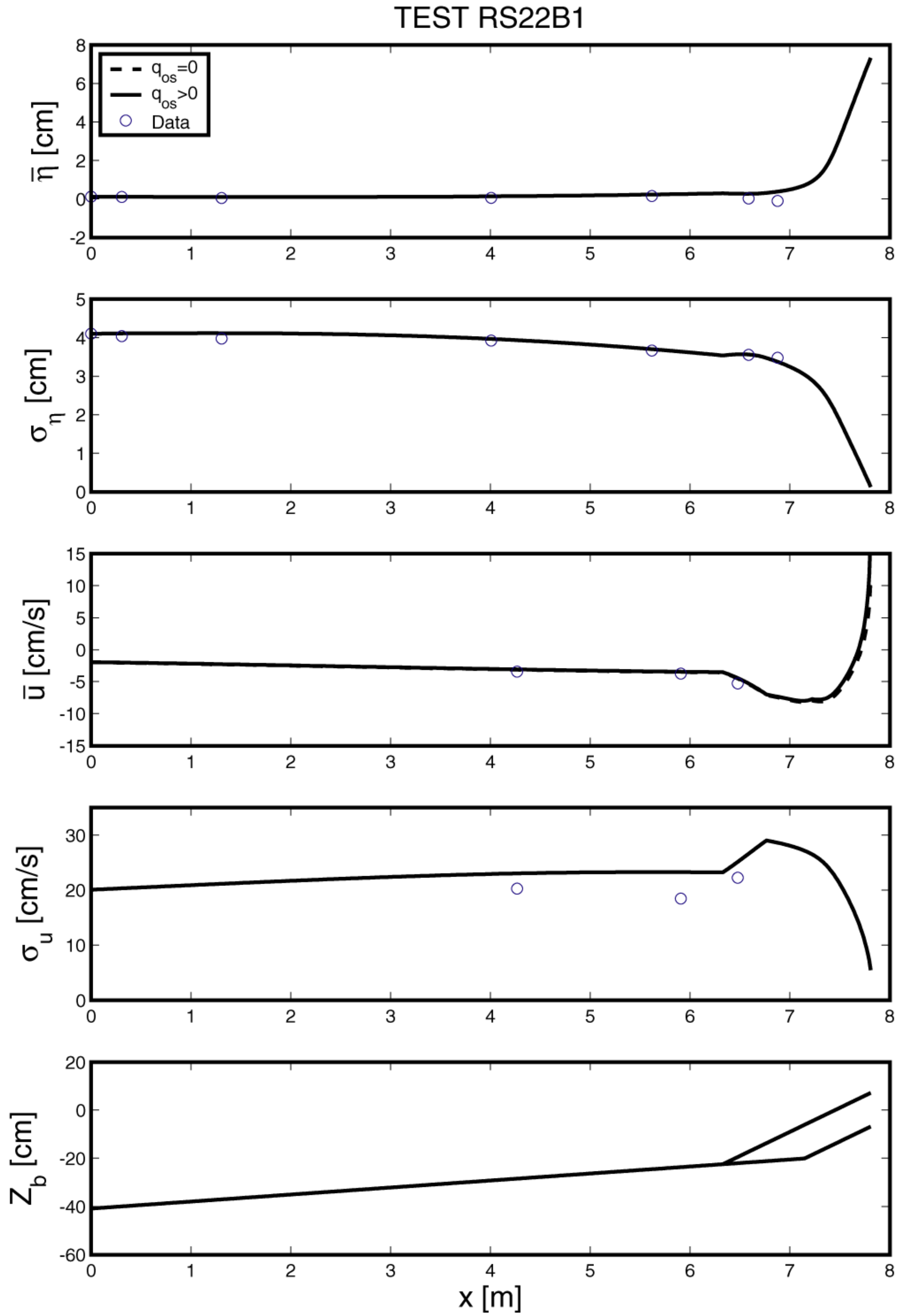

Fig. 16: Measured and predicted cross-shore variations of mean and standard variation of η and u above bottom profile z_b without ($q_{os} = 0$) and with ($q_{os} > 0$) combined overtopping and seepage rate for test RS22B1.

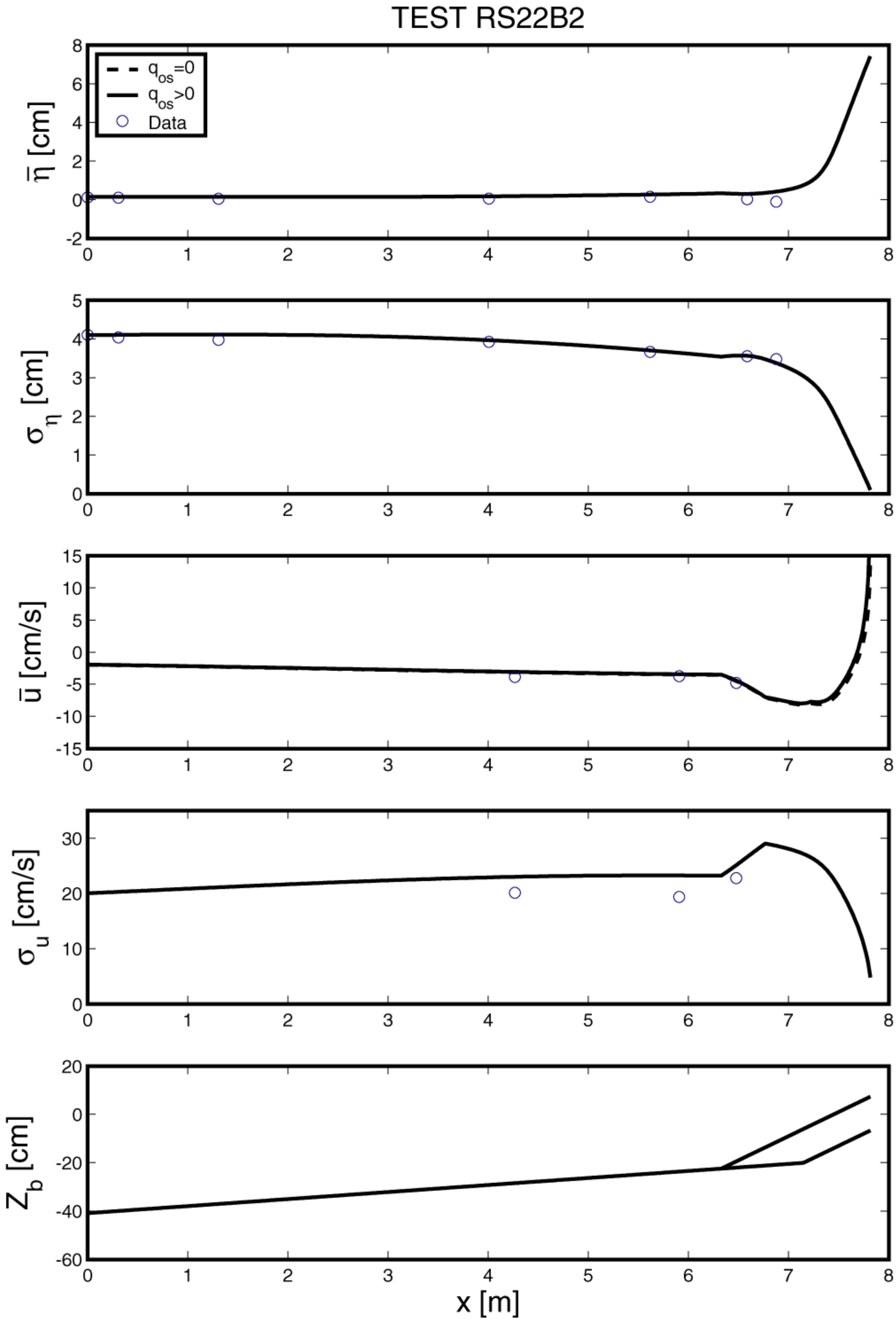

Fig. 17: Measured and predicted cross-shore variations of mean and standard variation of η and u above bottom profile z_b without ($q_{os}=0$) and with ($q_{os}>0$) combined overtopping and seepage rate for test RS22B2.

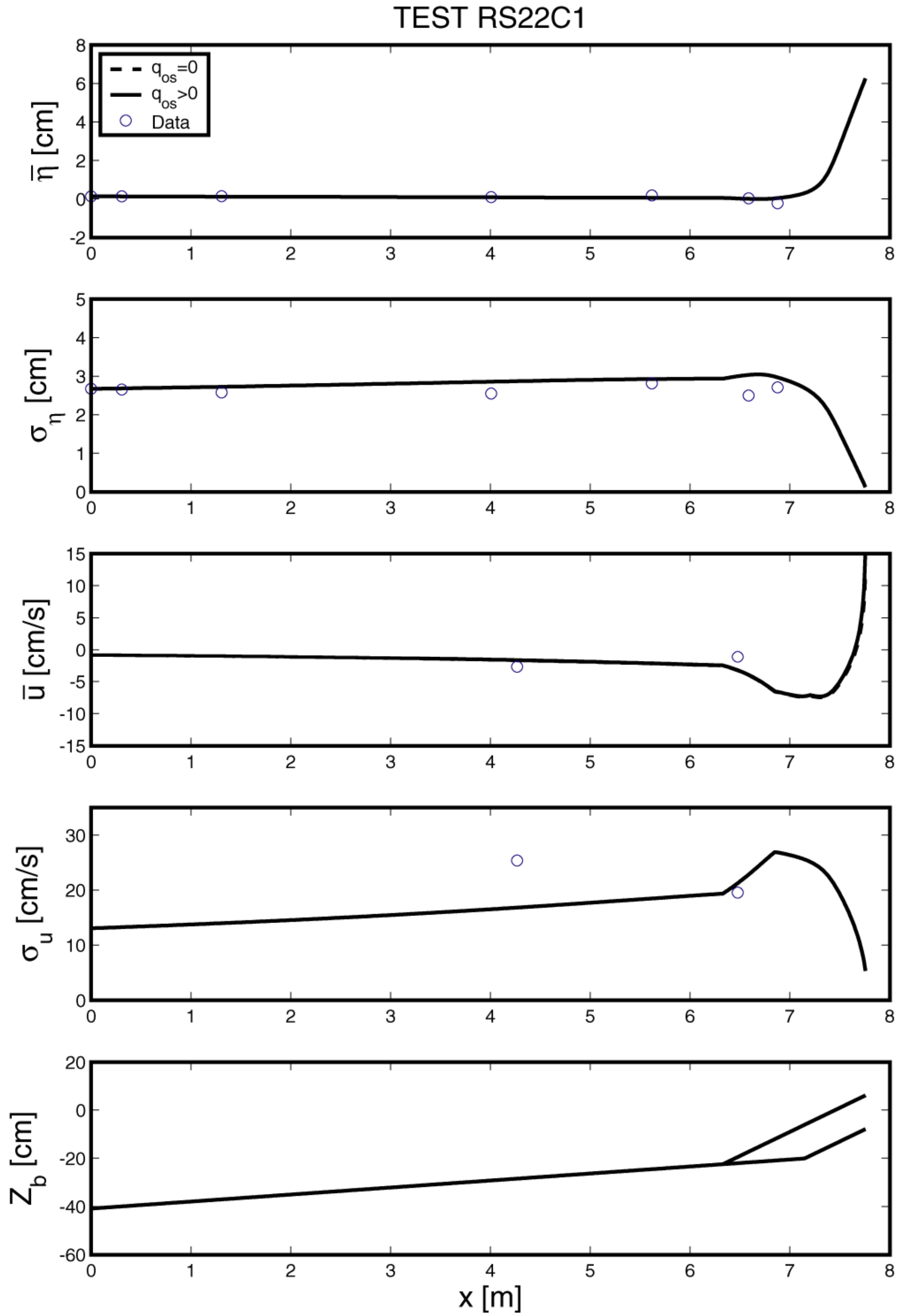

Fig. 18: Measured and predicted cross-shore variations of mean and standard variation of η and u above bottom profile z_b without ($q_{os} = 0$) and with ($q_{os} > 0$) combined overtopping and seepage rate for test RS22C1.

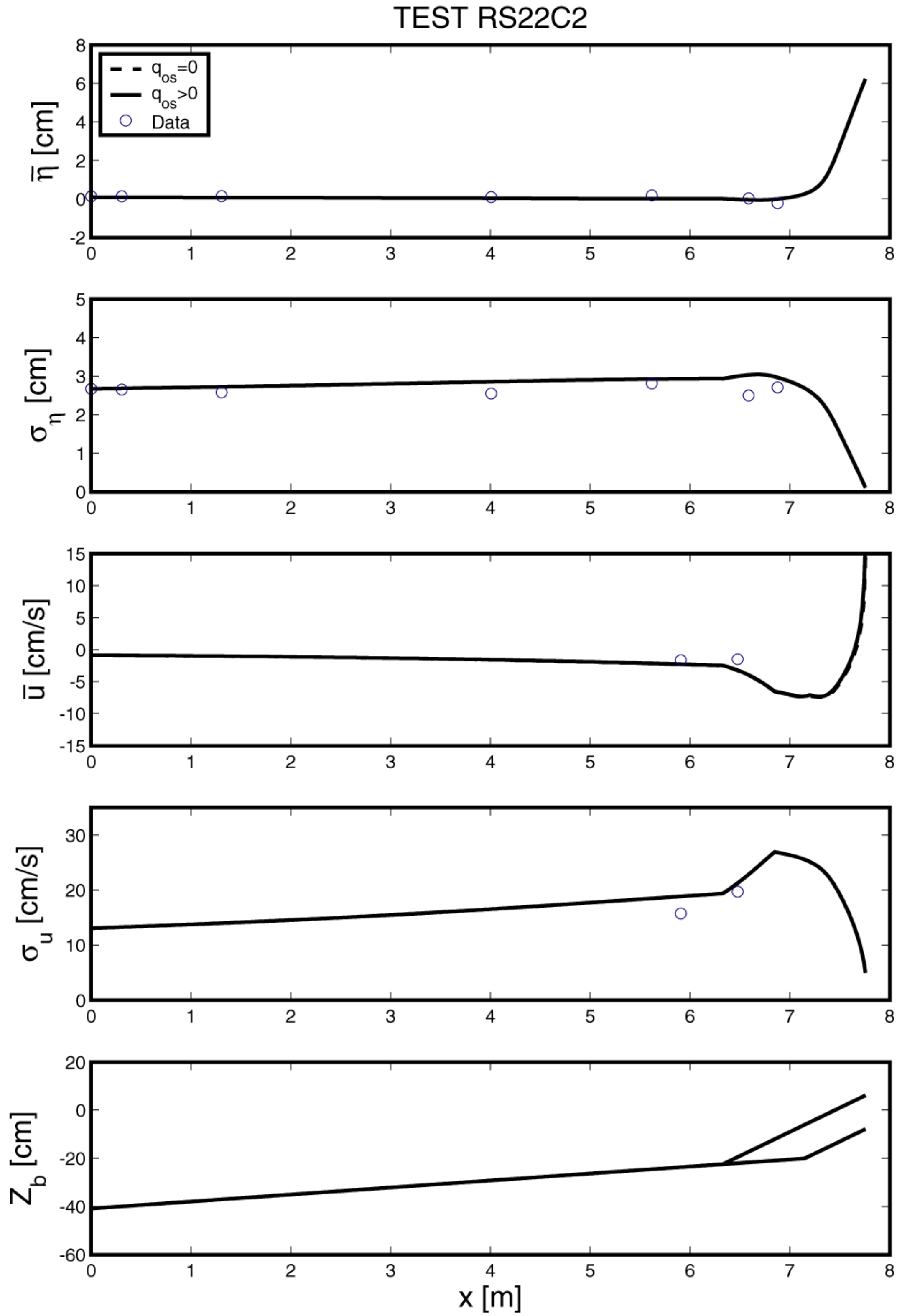

Fig. 19: Measured and predicted cross-shore variations of mean and standard variation of η and u above bottom profile z_b without ($q_{os} = 0$) and with ($q_{os} > 0$) combined overtopping and seepage rate for test RS22C2.

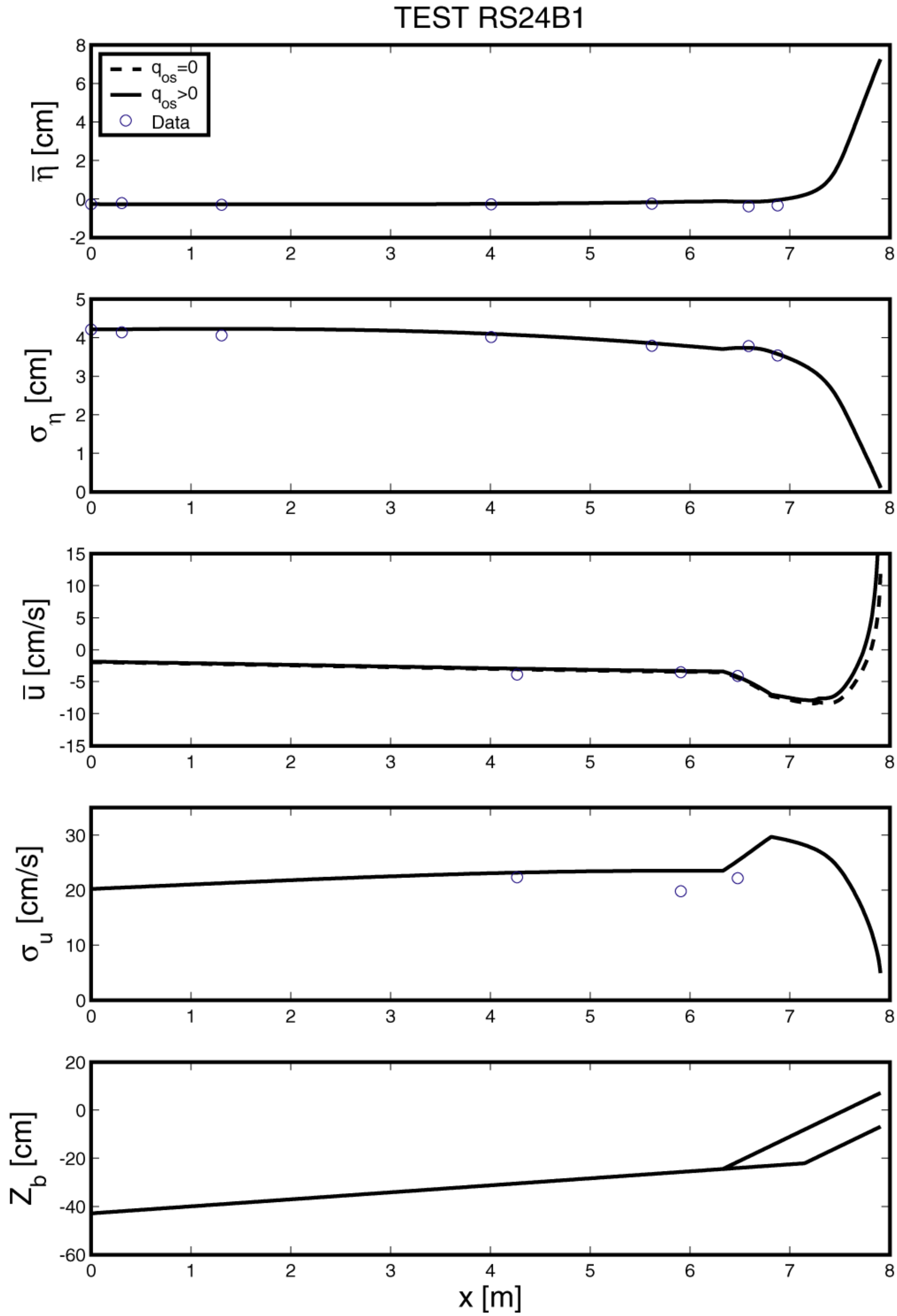

Fig. 20: Measured and predicted cross-shore variations of mean and standard variation of η and u above bottom profile z_b without ($q_{os} = 0$) and with ($q_{os} > 0$) combined overtopping and seepage rate for test RS24B1.

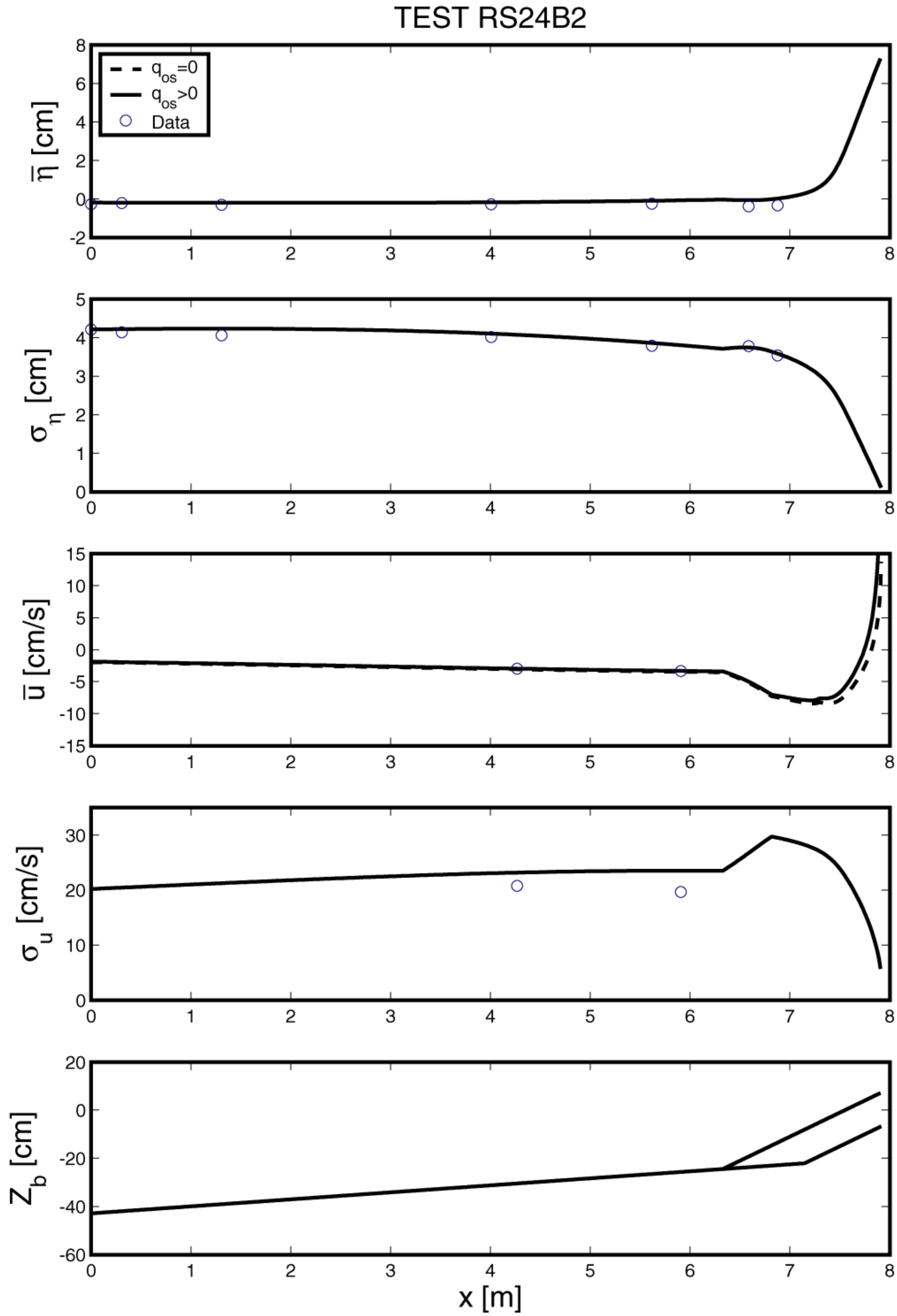

Fig. 21: Measured and predicted cross-shore variations of mean and standard variation of η and u above bottom profile z_b without ($q_{os} = 0$) and with ($q_{os} > 0$) combined overtopping and seepage rate for test RS24B2.

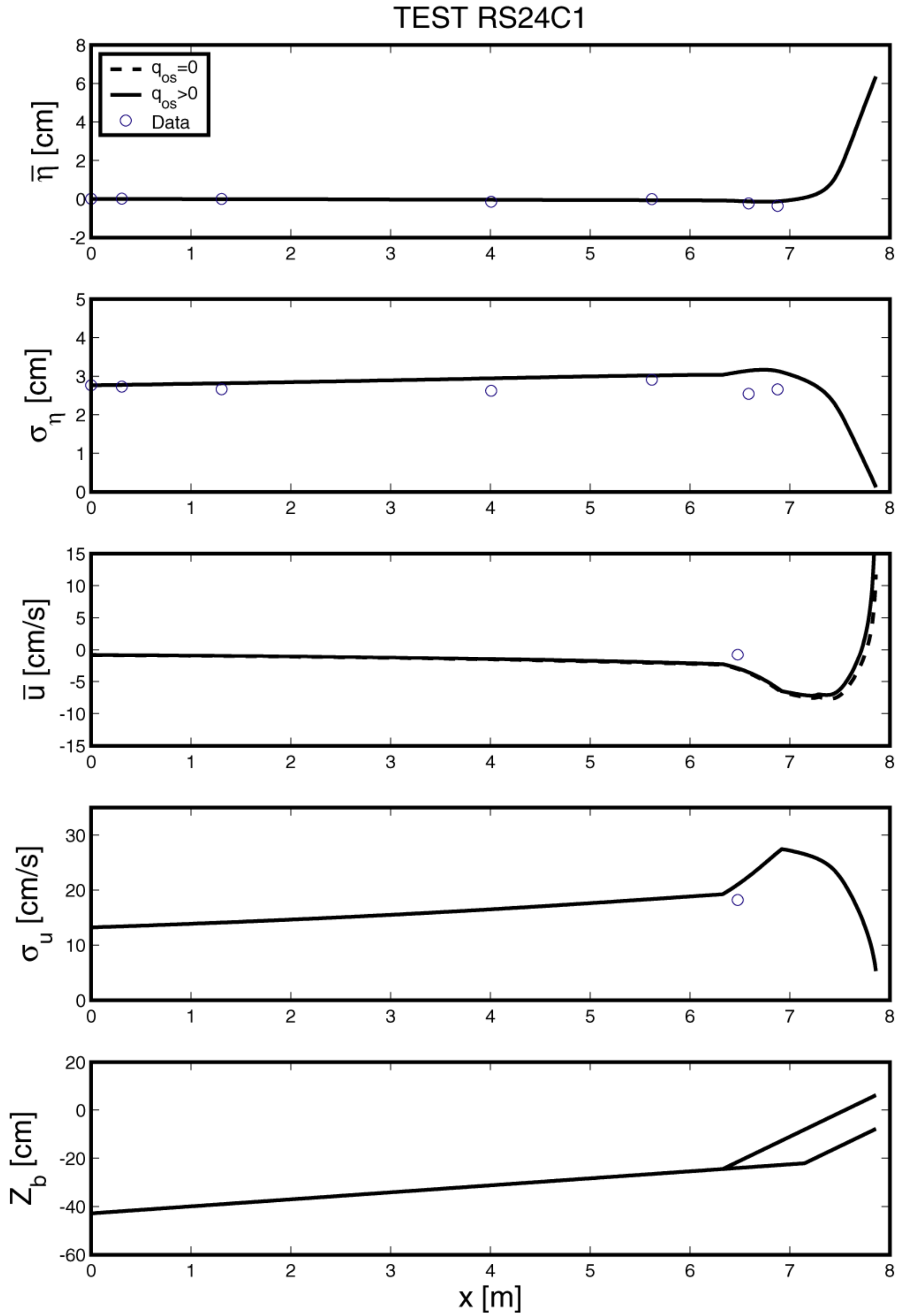

Fig. 22: Measured and predicted cross-shore variations of mean and standard variation of η and u above bottom profile z_b without ($q_{os} = 0$) and with ($q_{os} > 0$) combined overtopping and seepage rate for test RS24C1.

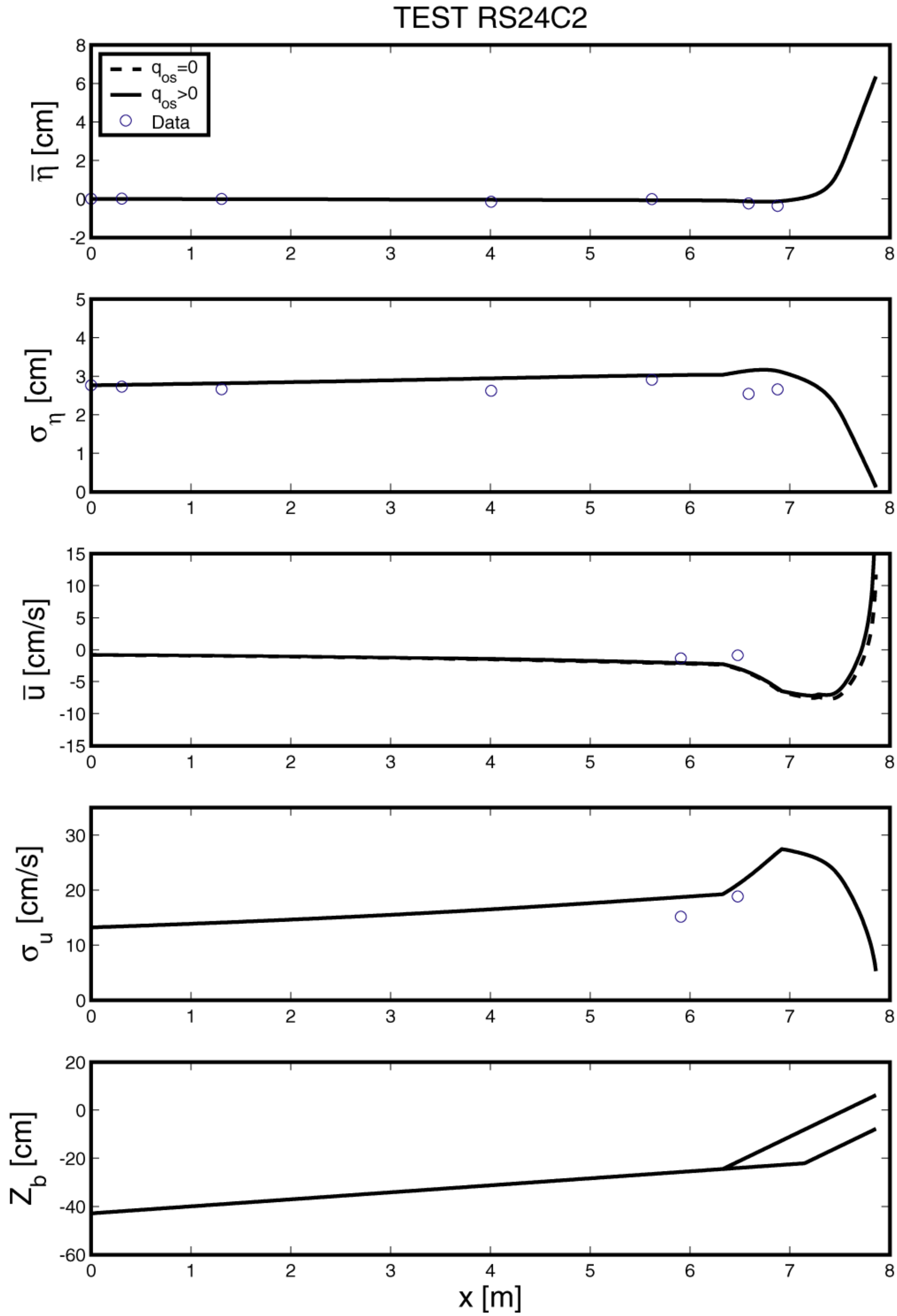

Fig. 23: Measured and predicted cross-shore variations of mean and standard variation of η and u above bottom profile z_b without ($q_{os} = 0$) and with ($q_{os} > 0$) combined overtopping and seepage rate for test RS24C2.

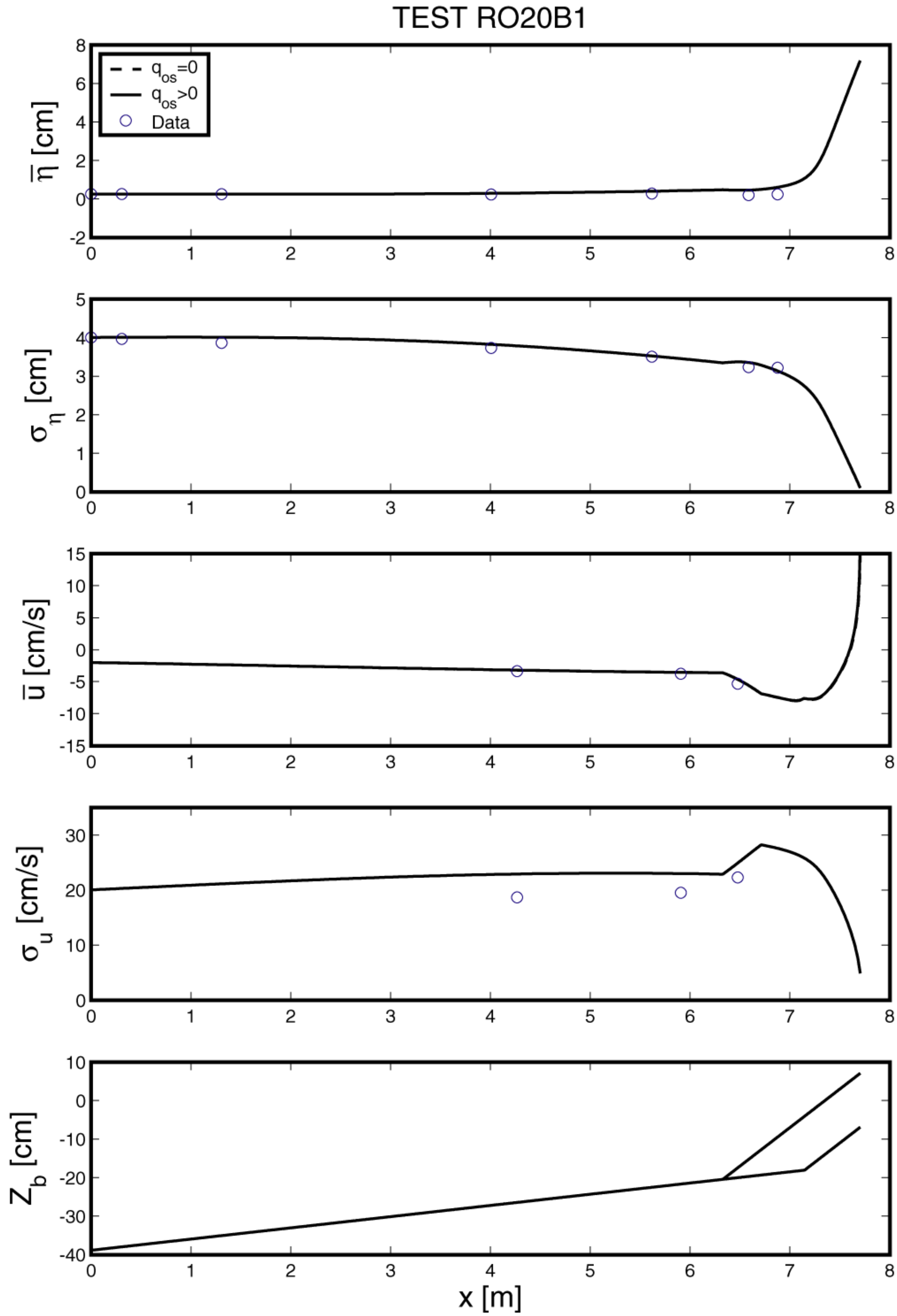

Fig. 24: Measured and predicted cross-shore variations of mean and standard variation of η and u above bottom profile z_b without ($q_{os} = 0$) and with ($q_{os} > 0$) combined overtopping and seepage rate for test RO20B1.

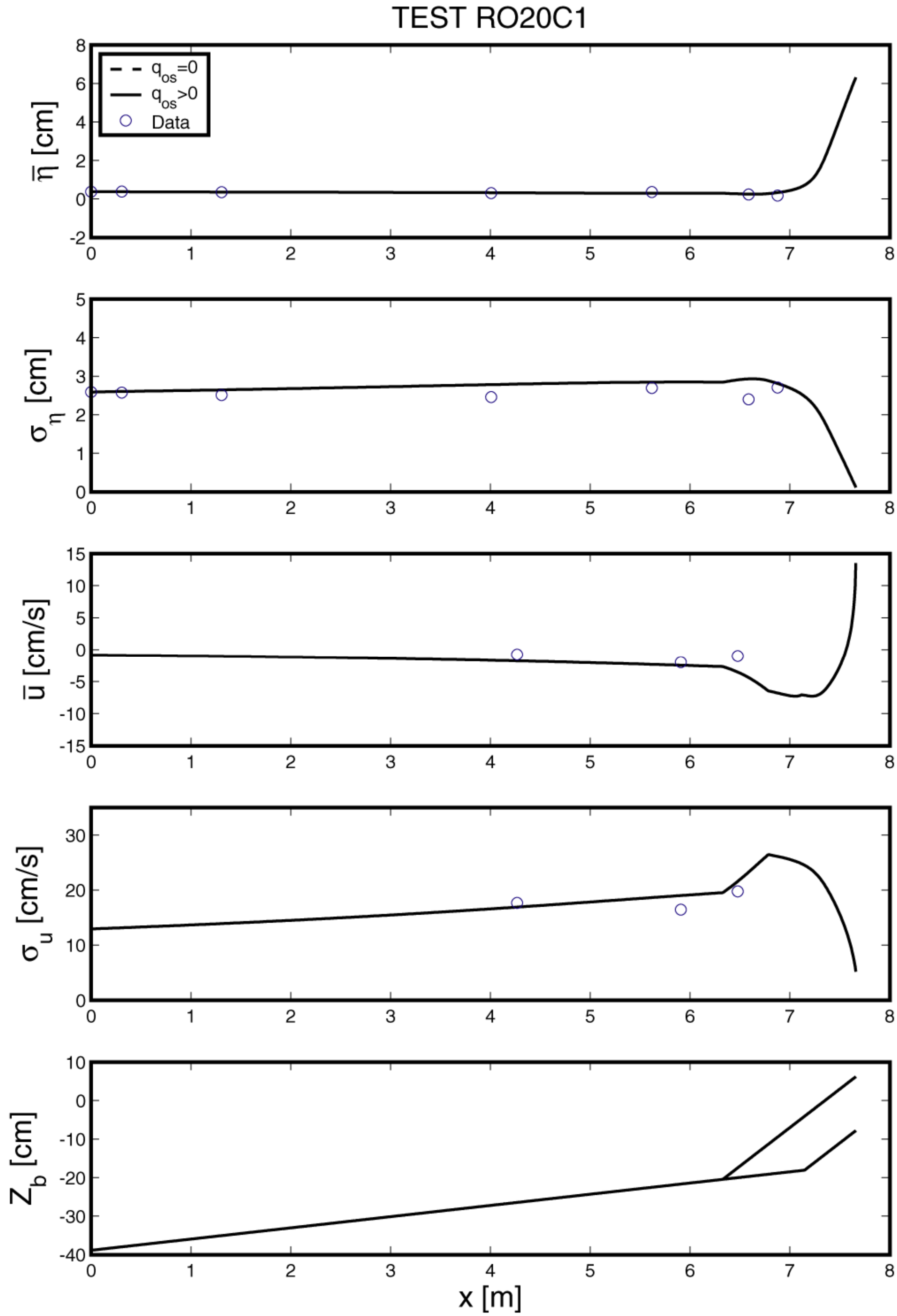

Fig. 25: Measured and predicted cross-shore variations of mean and standard variation of η and u above bottom profile z_b without ($q_{os} = 0$) and with ($q_{os} > 0$) combined overtopping and seepage rate for test RO20C1.

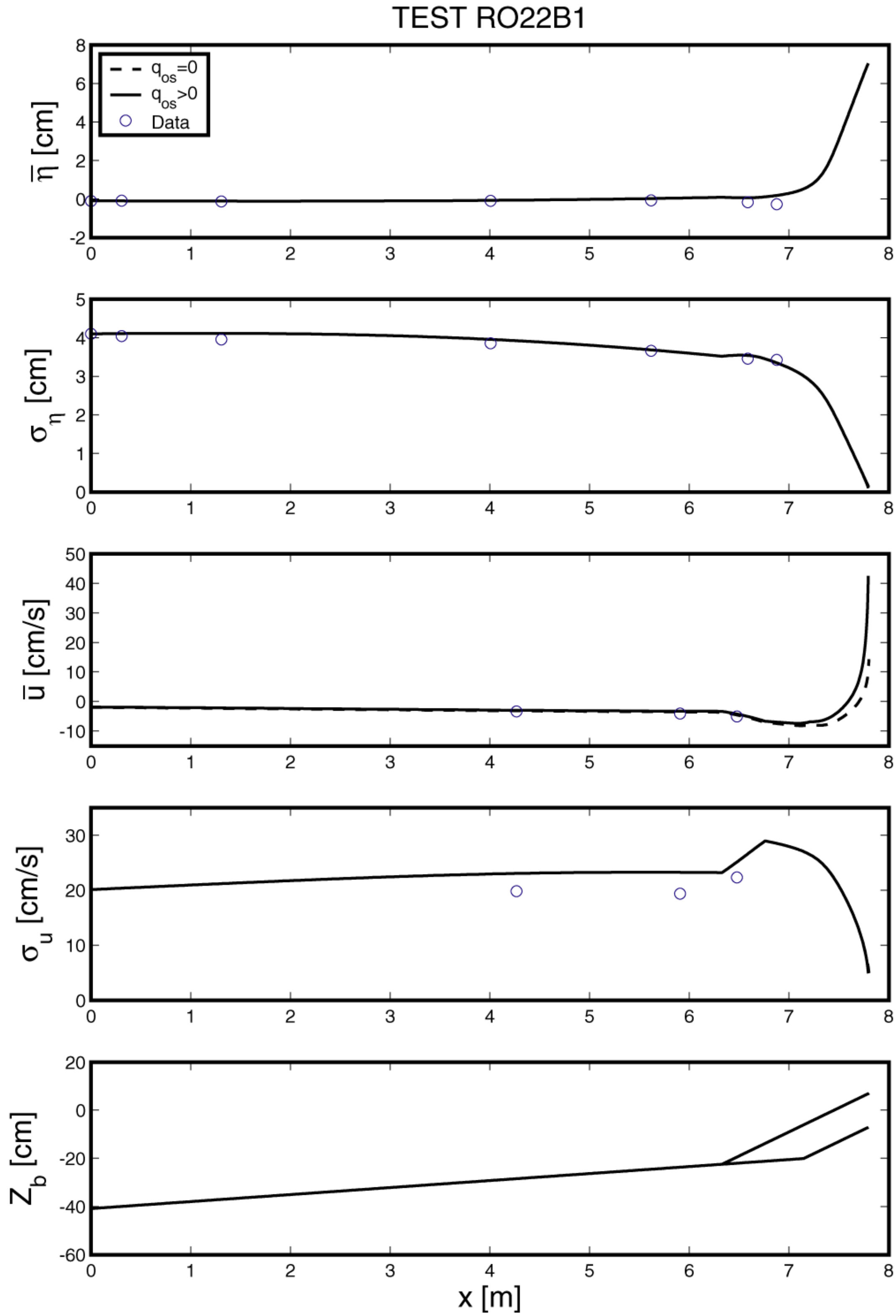

Fig. 26: Measured and predicted cross-shore variations of mean and standard variation of η and u above bottom profile z_b without ($q_{os} = 0$) and with ($q_{os} > 0$) combined overtopping and seepage rate for test RO22B1.

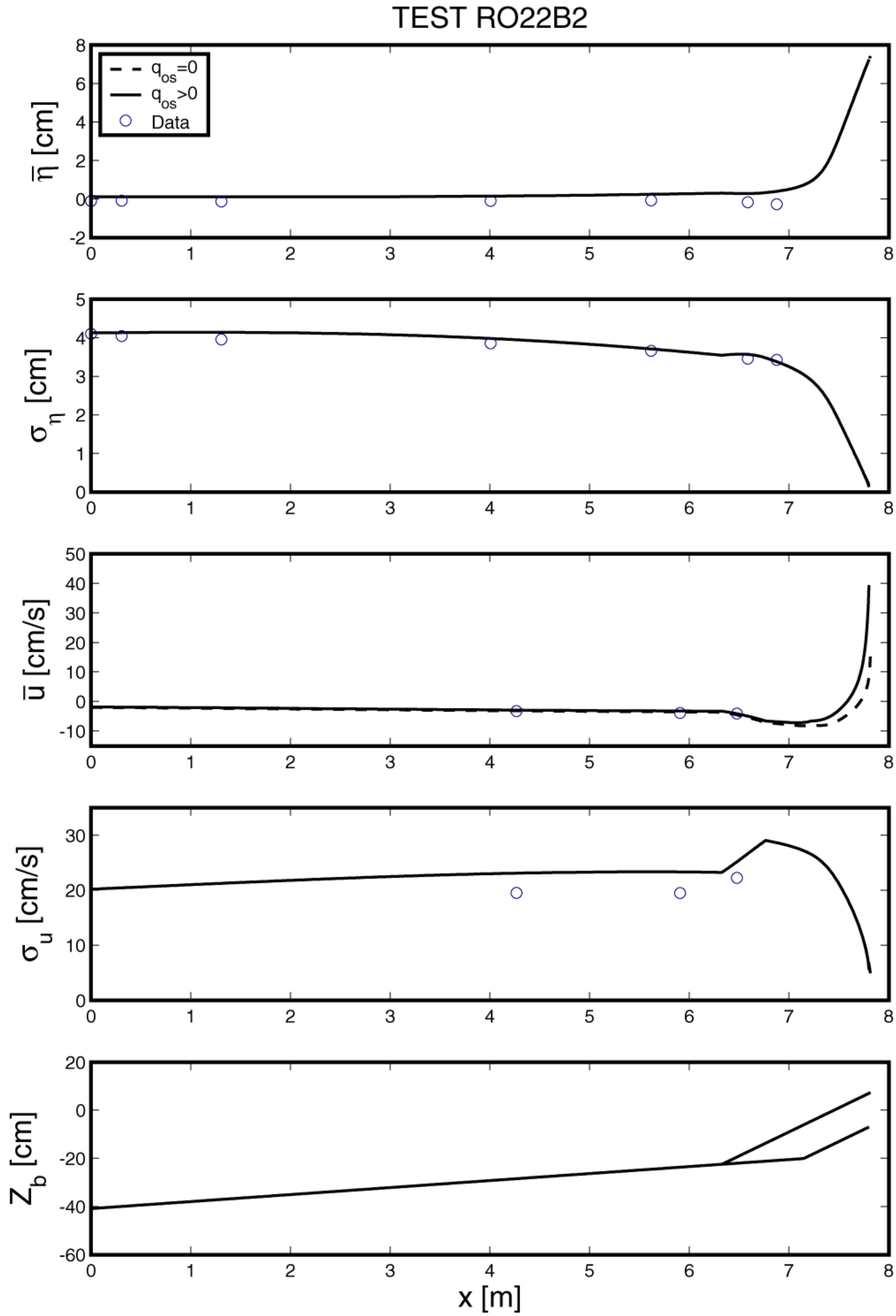

Fig. 27: Measured and predicted cross-shore variations of mean and standard variation of η and u above bottom profile z_b without ($q_{os} = 0$) and with ($q_{os} > 0$) combined overtopping and seepage rate for test RO22B2.

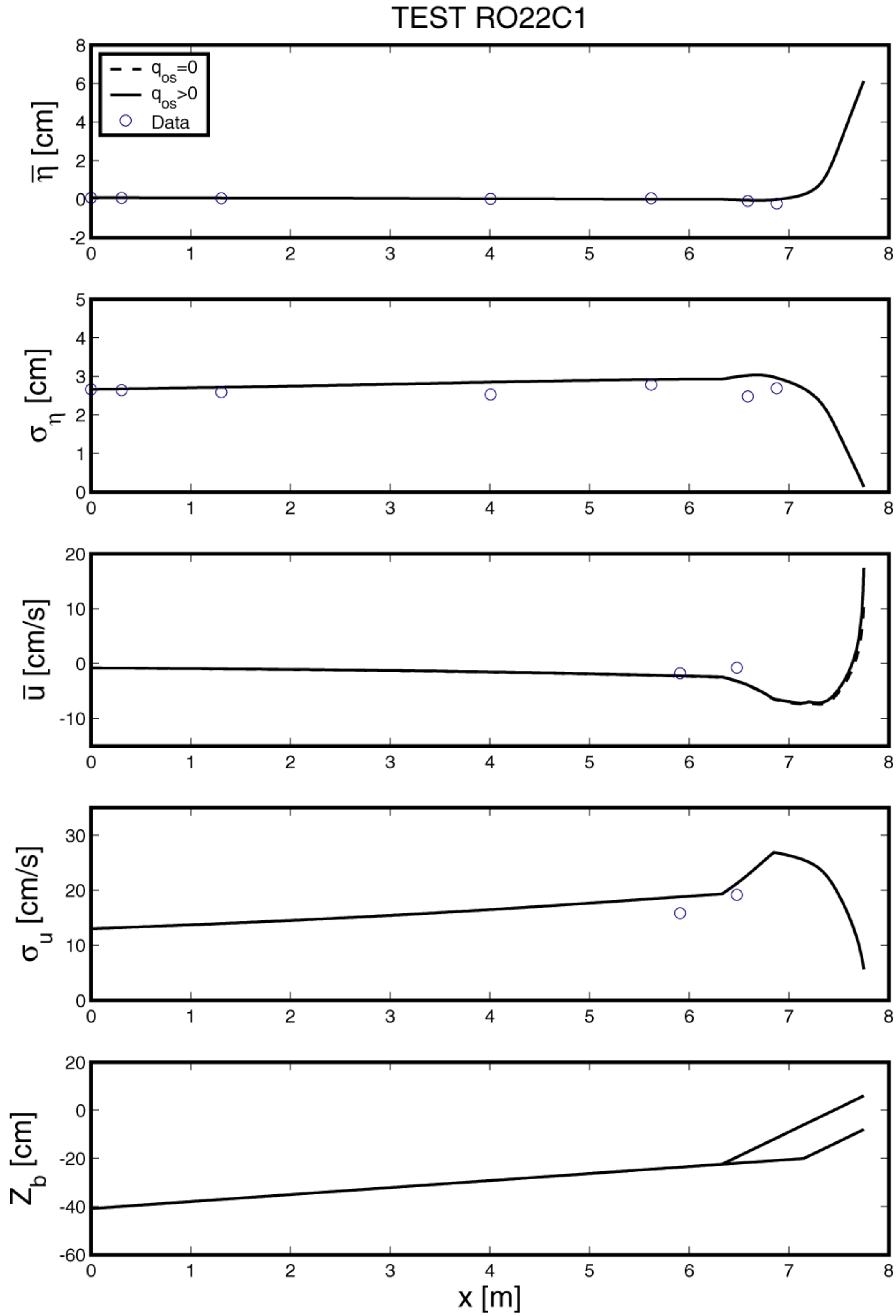

Fig. 28: Measured and predicted cross-shore variations of mean and standard variation of η and u above bottom profile z_b without ($q_{os} = 0$) and with ($q_{os} > 0$) combined overtopping and seepage rate for test RO22C1.

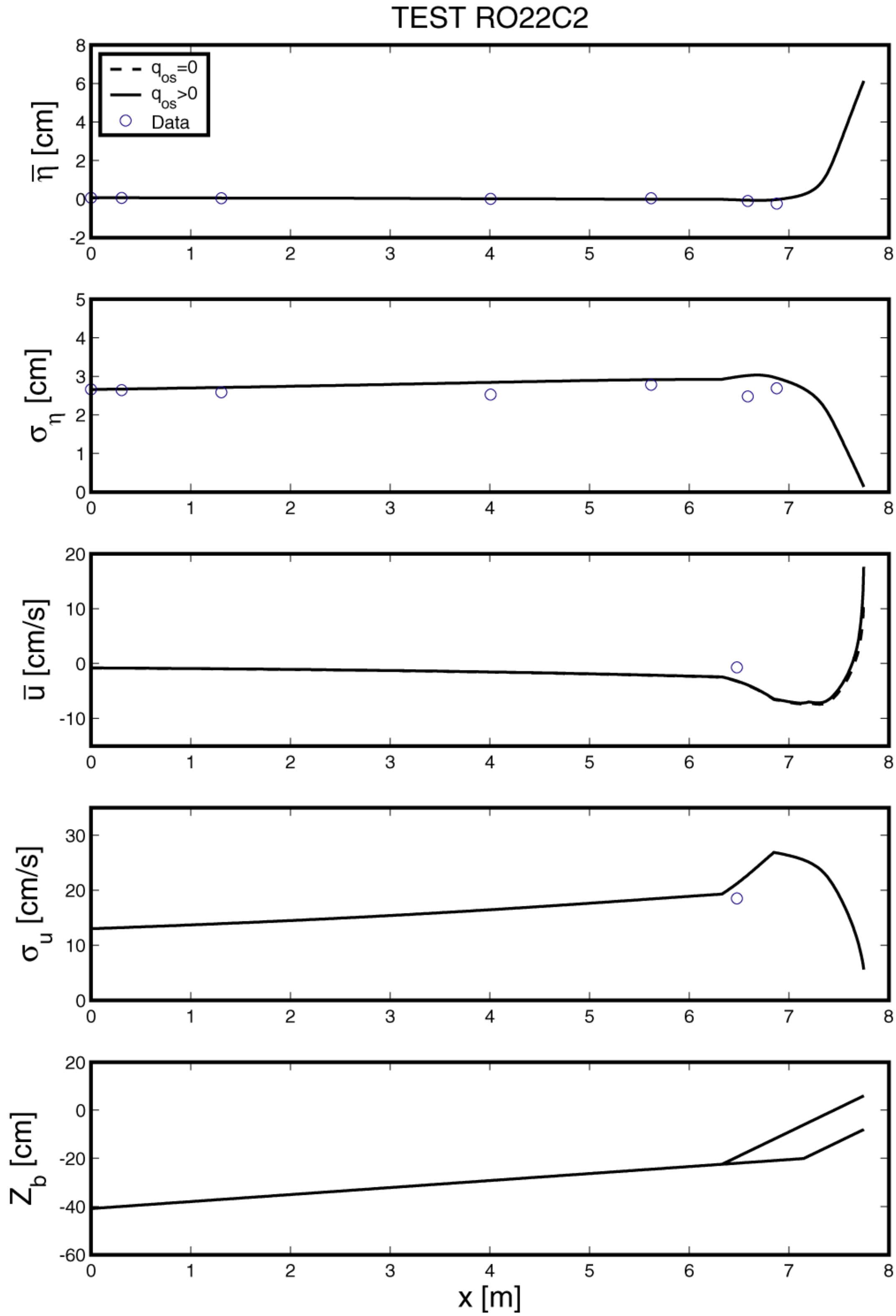

Fig. 29: Measured and predicted cross-shore variations of mean and standard variation of η and u above bottom profile z_b without ($q_{os} = 0$) and with ($q_{os} > 0$) combined overtopping and seepage rate for test RO22C2.

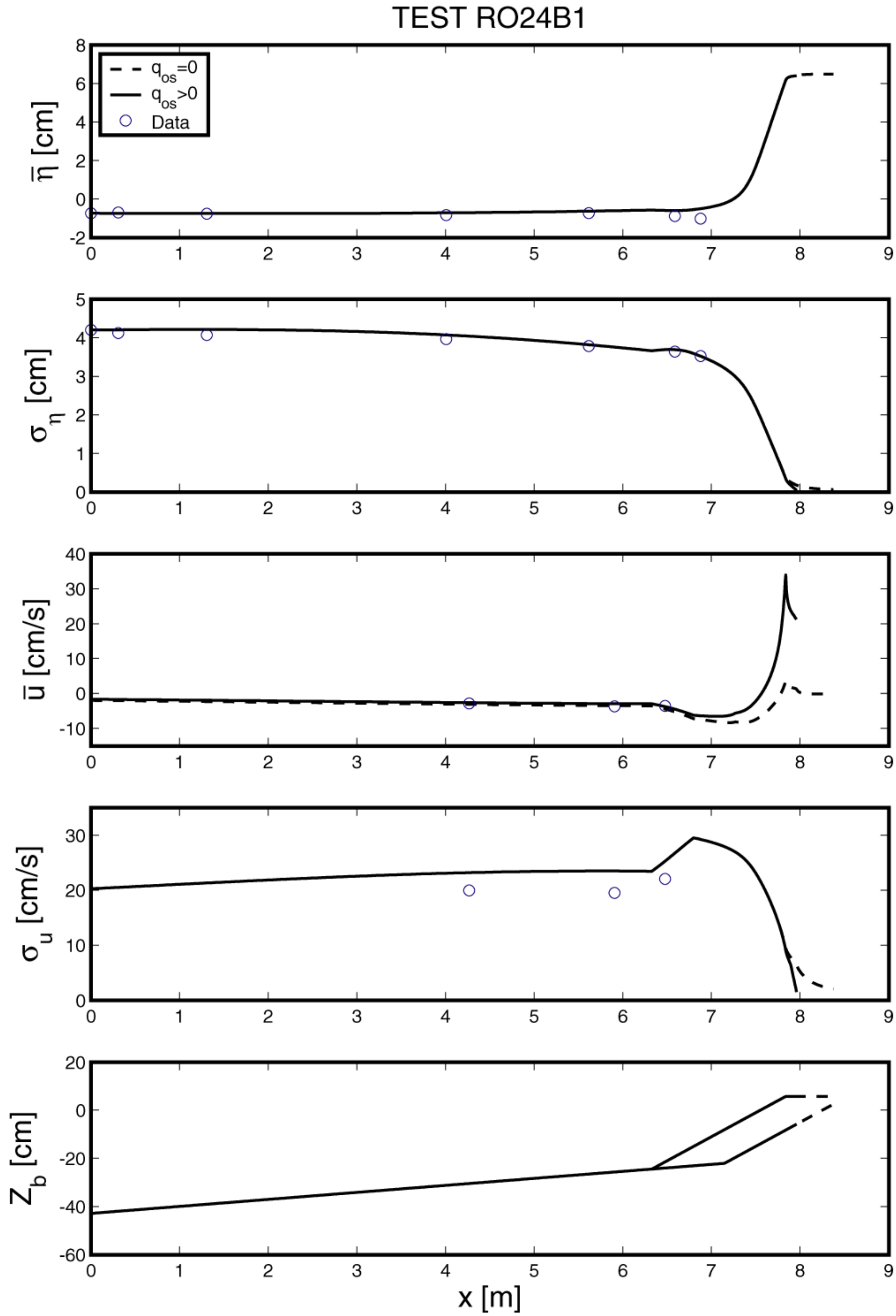

Fig. 30: Measured and predicted cross-shore variations of mean and standard variation of η and u above bottom profile z_b without ($q_{os} = 0$) and with ($q_{os} > 0$) combined overtopping and seepage rate for test RO24B1.

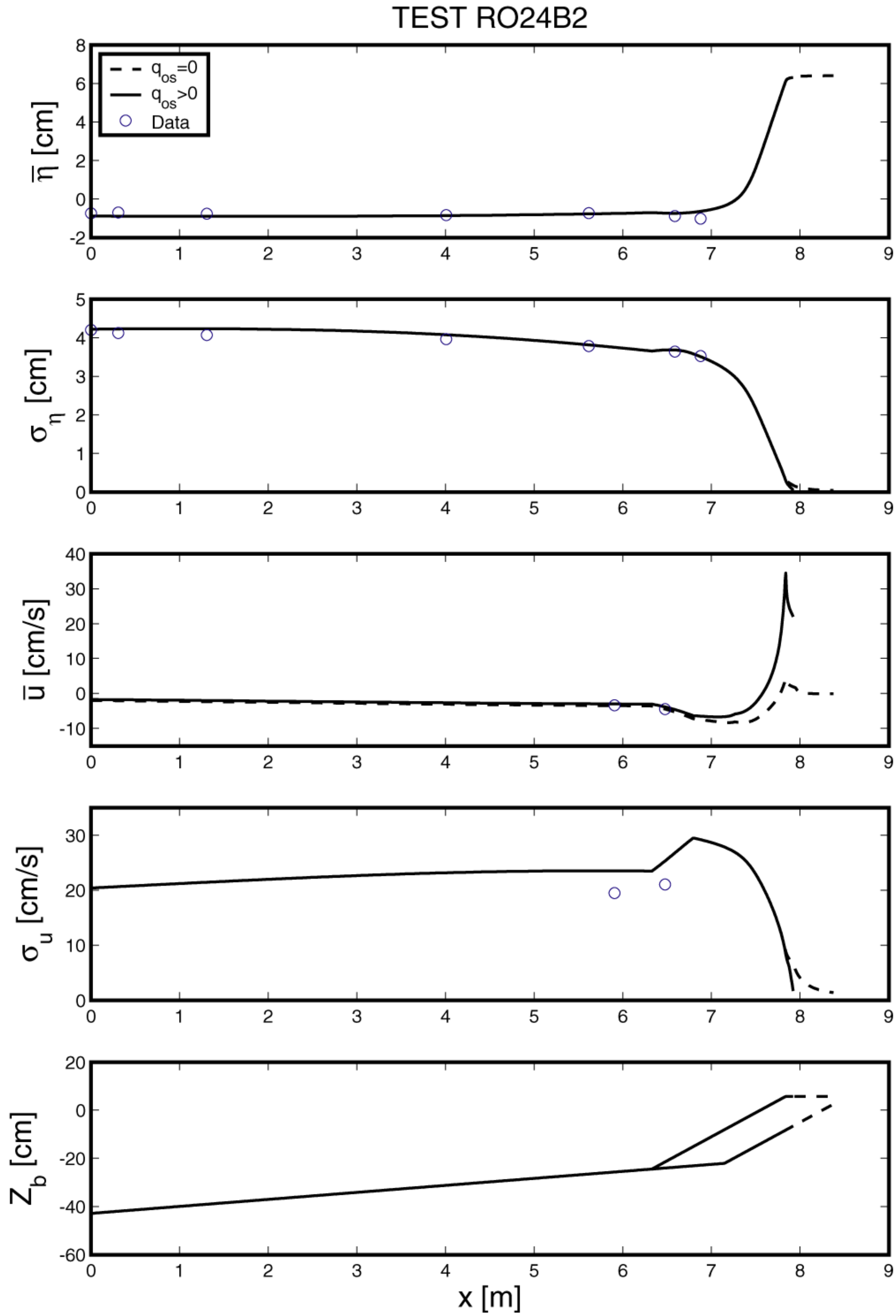

Fig. 31: Measured and predicted cross-shore variations of mean and standard variation of η and u above bottom profile z_b without ($q_{os} = 0$) and with ($q_{os} > 0$) combined overtopping and seepage rate for test RO24B2.

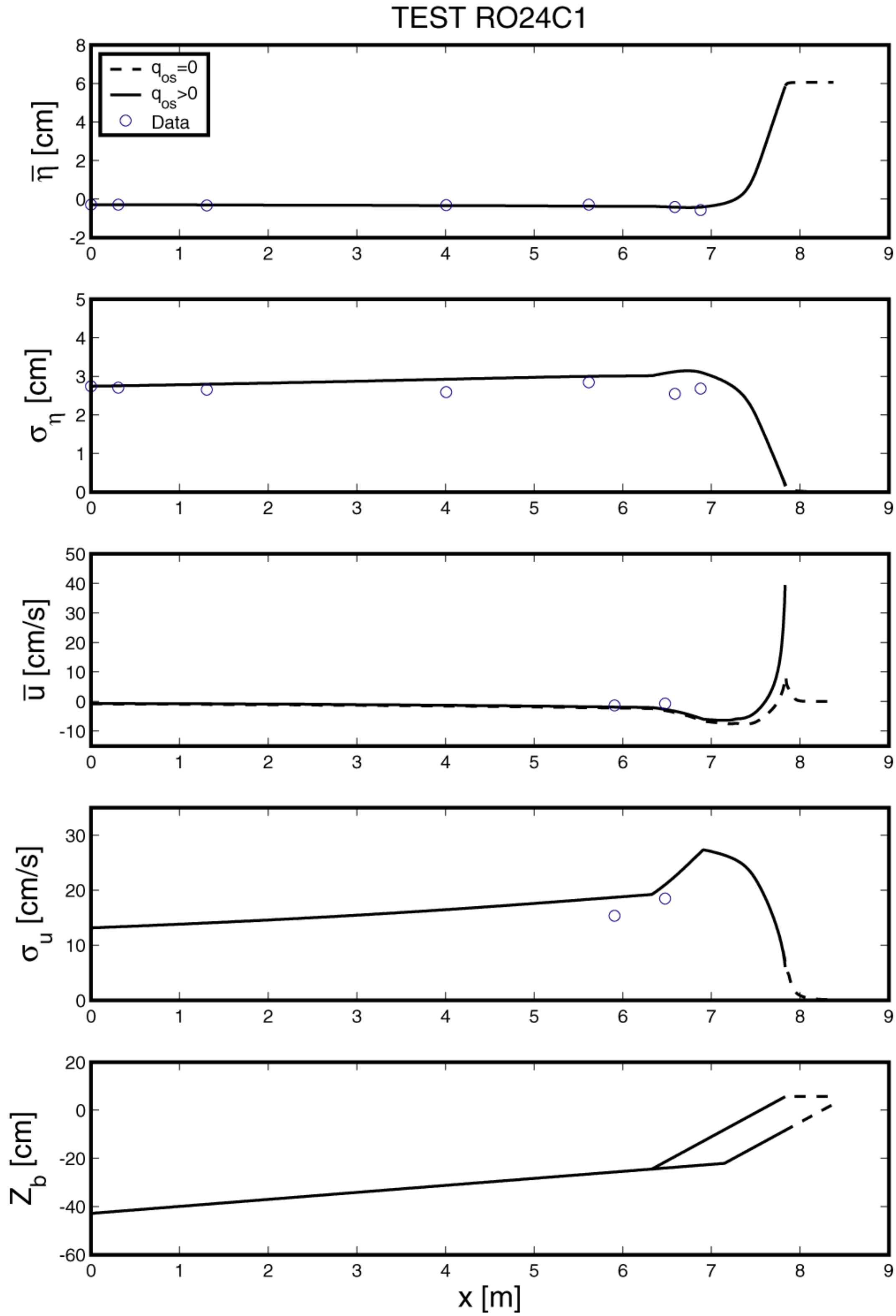

Fig. 32: Measured and predicted cross-shore variations of mean and standard variation of η and u above bottom profile z_b without ($q_{os} = 0$) and with ($q_{os} > 0$) combined overtopping and seepage rate for test RO24C1.

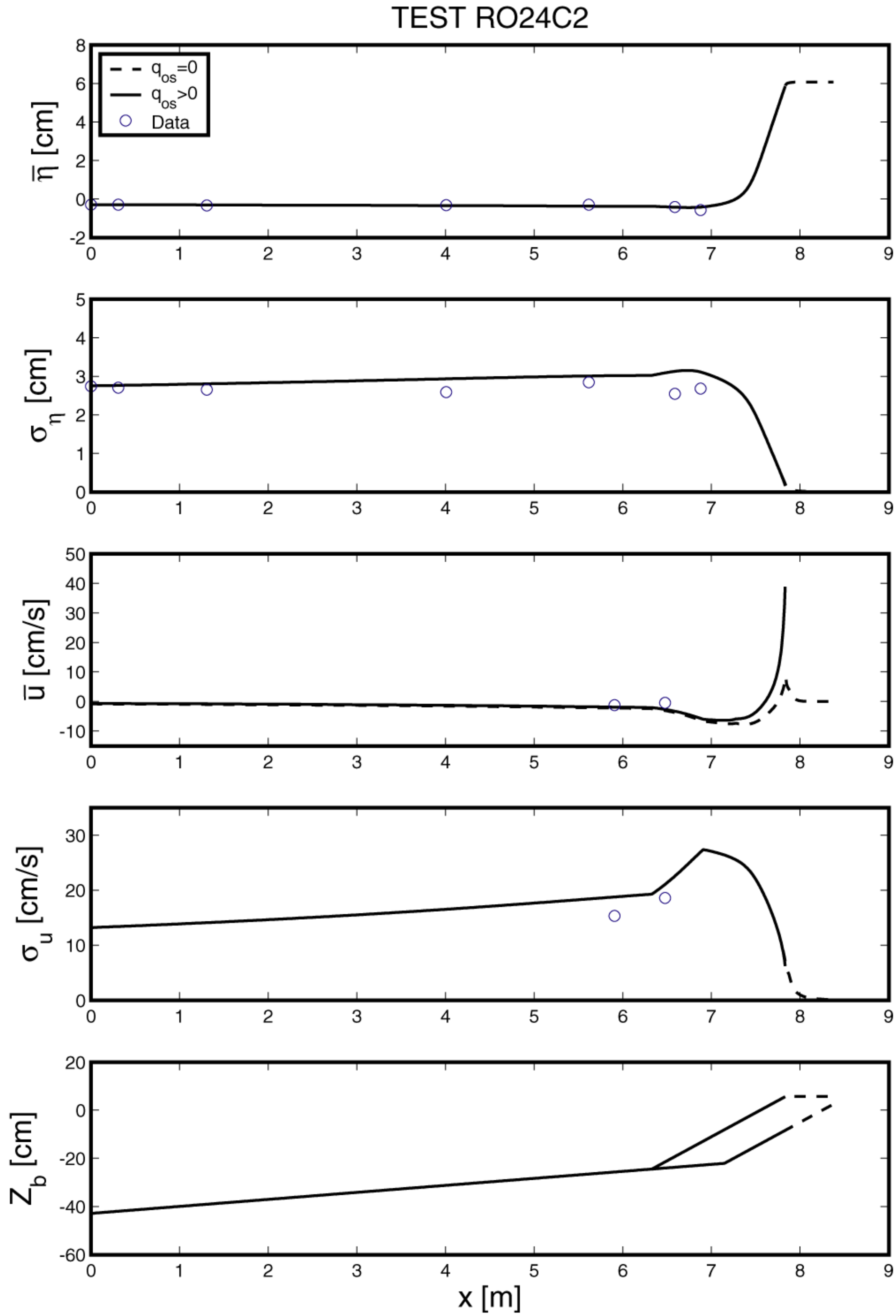

Fig. 33: Measured and predicted cross-shore variations of mean and standard variation of η and u above bottom profile z_b without ($q_{os}=0$) and with ($q_{os}>0$) combined overtopping and seepage rate for test RO24C2.

4.2 WAVE RUNUP STATISTICS

Fig. 34 compares the measured and predicted values of the mean $\overline{\eta_r}$ of the shoreline elevation η_r for the S and OS tests. The model overpredicts $\overline{\eta_r}$ for almost all the tests. This is partly because the model does not account for the small decrease of the still water level in the wave flume due to the water collected in the overtopping tank. Fig. 35 shows the comparison of the measured and predicted standard deviation σ_r of the shoreline elevation for the S and OS tests. The agreement is fair and the model can predict σ_r within the error of 20%. The same trend was observed by de los Santos and Kobayashi (2005) for the comparisons with runup tests with no seepage and no overtopping.

Fig. 36 compares the measured and predicted significant runup heights $R_{1/3}$ for the S and OS tests. Eq. (5) developed for the case of no seepage and no overtopping predicts $R_{1/3}$ within the error of about 20%.

Fig. 37 compares the measured and predicted runup heights $R_{2\%}$ for the 2% exceedance probability where Eq. (3) yields

$$R_{2\%} = \overline{\eta_r} + (1.40)^{2/\kappa} \left(R_{1/3} - \overline{\eta_r} \right) \tag{21}$$

where the shape parameter κ given by Eq. (2) accounts for the decrease of $R_{2\%}$ due to the decrease of the normalized crest height R_* and the resulting increase of the wave overtopping probability P_o given by Eq.(4). The empirical formula of van der Meer and Janssen (1995) is also compared with the data. For the case of normally incident waves on a slope with no berm, this formula can be expressed as

$$R_{2\%} = 1.5 \xi \gamma_f \gamma_h H_{1/3} \qquad \text{with} \qquad \xi \le 2 \tag{22}$$

with

$$\xi = \left(\frac{gT_p^2}{2\pi H_{1/3}} \right)^{0.5} \tan\theta \quad ; \quad \gamma_h = 1 - 0.03 \left(4 - \frac{d_t}{H_{1/3}} \right)^2 \quad \text{if} \quad \frac{d_t}{H_{1/3}} < 4 \tag{23}$$

where ξ = surf similarity parameter; $H_{1/3}$ = significant wave height at the toe of the slope; γ_f = reduction factor due to slope roughness; γ_h = reduction factor due to wave breaking on a shallow foreshore which is less than unity if $(d_t / H_{1/3}) < 4$. Eq. (22) implies that (1.5 ξ) is replaced by 3.0 if ξ > 2. The reduction factor γ_h based on the measured ratio, $H_{2\%} / (1.4 H_{1/3})$, on a foreshore slope of 1/100 with $H_{2\%}$ = 2% exceedance wave height is assumed to be valid for the present beach slope of 1/34.4. The reduction factor γ_f for a rubble layer with two or more stone diameter thickness was suggested to be in the range of 0.50 – 0.55 for $\xi < 4$ and γ_f = 0.52 is used here. The significant wave height $H_{1/3}$ for each test is obtained from the time series of the free surface elevation measured by the wave gauge at the toe of the slope. For the S and OS tests, 1.4 $< \xi <$ 2.4 and 0.79 $< \gamma_h <$ 0.89. All the parameters for the S and OS tests are summarized in Table 6 and Table 7, respectively. Fig. 37 indicates that the numerical model predicts $R_{2\%}$ within the error of about 20%, partly because Eq. (21) is devised using the same S and OS tests. It is also shown that the empirical formula overpredicts $R_{2\%}$ for the OS tests. This is because this formula was developed for no or minor overtopping. It should be noted that the numerical model uses the measured H_{rms} outside the surf zone instead of the measured $H_{1/3}$ at the toe of the slope unlike the empirical formula.

Table 6: Comparison with empirical formula for $R_{2\%}$ for S tests.

Test	d_t $[cm]$	$H_{1/3}$ $[cm]$	T_p $[s]$	ξ	γ_h	γ_f	Empirical $R_{2\%}$ $[cm]$	Measured $R_{2\%}$ $[cm]$
RS20B1	20.5	14.90	2.3	1.5	0.79	0.52	13.73	13.31
RS20B2	20.5	14.59	2.3	1.5	0.80	0.52	13.67	13.91
RS20C1	20.5	11.09	3.0	2.3	0.86	0.52	14.89	13.59
RS20C2	20.5	11.90	3.0	2.2	0.85	0.52	15.68	14.03
RS22B1	22.5	15.56	2.3	1.5	0.81	0.52	14.22	14.07
RS22B2	22.5	15.63	2.3	1.5	0.80	0.52	14.24	14.44
RS22C1	22.5	12.09	2.9	2.1	0.86	0.52	16.27	14.60
RS22C2	22.5	11.58	2.9	2.1	0.87	0.52	15.77	14.60
RS24B1	24.5	16.91	2.3	1.4	0.81	0.52	14.84	14.12
RS24B2	24.5	15.95	2.3	1.4	0.82	0.52	14.64	15.66
RS24C1	24.5	11.77	2.9	2.1	0.89	0.52	16.34	14.98
RS24C2	24.5	11.64	2.9	2.1	0.89	0.52	16.20	14.71

Table 7: Comparison with empirical formula for $R_{2\%}$ for OS tests.

Test	d_t $[cm]$	$H_{1/3}$ $[cm]$	T_p $[s]$	ξ	γ_h	γ_f	Empirical $R_{2\%}$ $[cm]$	Measured $R_{2\%}$ $[cm]$
RO20B1	20.5	14.45	2.3	1.5	0.80	0.52	13.69	13.36
RO20C1	20.5	10.19	3.0	2.4	0.88	0.52	14.02	12.95
RO22B1	22.5	14.42	2.3	1.5	0.82	0.52	14.04	11.87
RO22B2	22.5	13.80	2.3	1.6	0.83	0.52	13.91	11.74
RO22C1	22.5	12.03	2.9	2.1	0.86	0.52	16.22	11.50
RO22C2	22.5	11.94	2.9	2.1	0.87	0.52	16.12	11.88
RO24B1	24.5	15.69	2.3	1.5	0.82	0.52	14.65	10.04
RO24B2	24.5	16.30	2.3	1.4	0.81	0.52	14.78	10.82
RO24C1	24.5	12.25	2.9	2.1	0.88	0.52	16.82	10.26
RO24C2	24.5	12.08	2.9	2.1	0.88	0.52	16.64	10.33

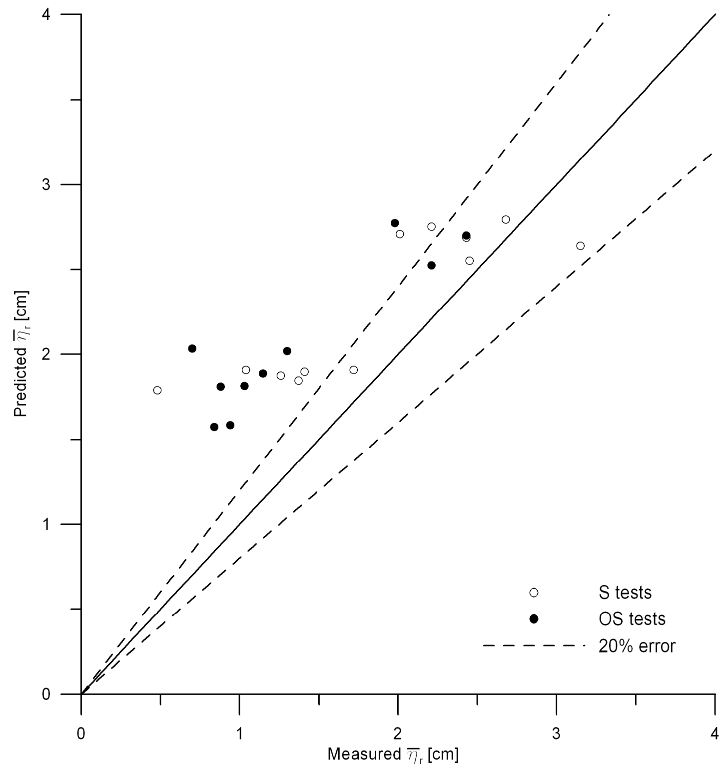

Fig. 34: Measured and predicted mean shoreline elevation $\overline{\eta_r}$ for all S and OS tests.

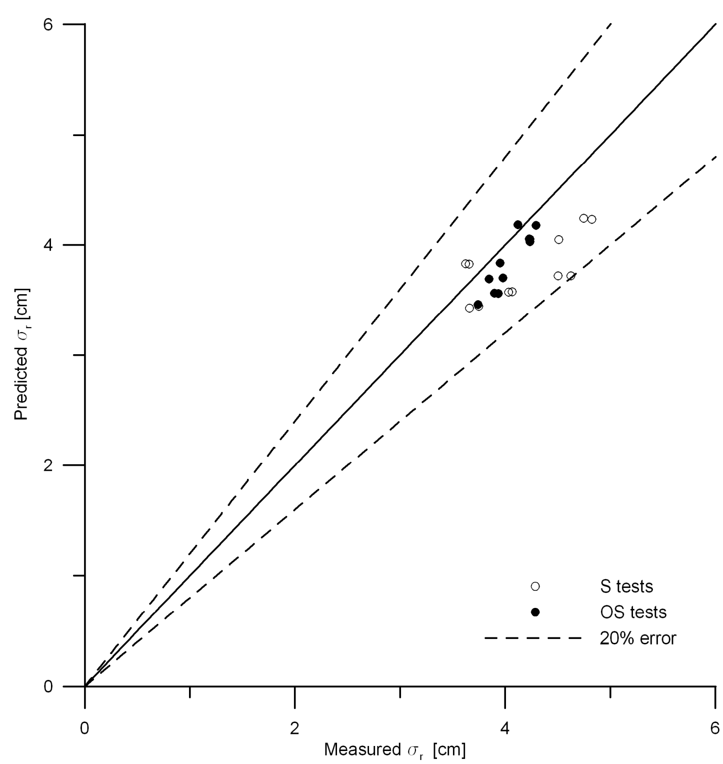

Fig. 35: Measured and predicted standard dev. of shoreline oscillations σ_r for S and OS tests.

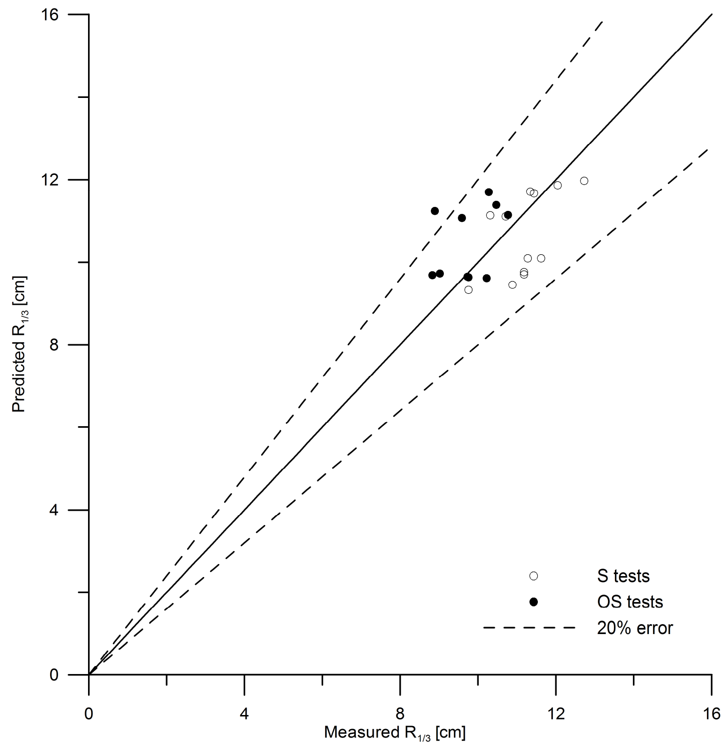

Fig. 36: Measured and predicted significant runup heights $R_{1/3}$ for S and OS tests.

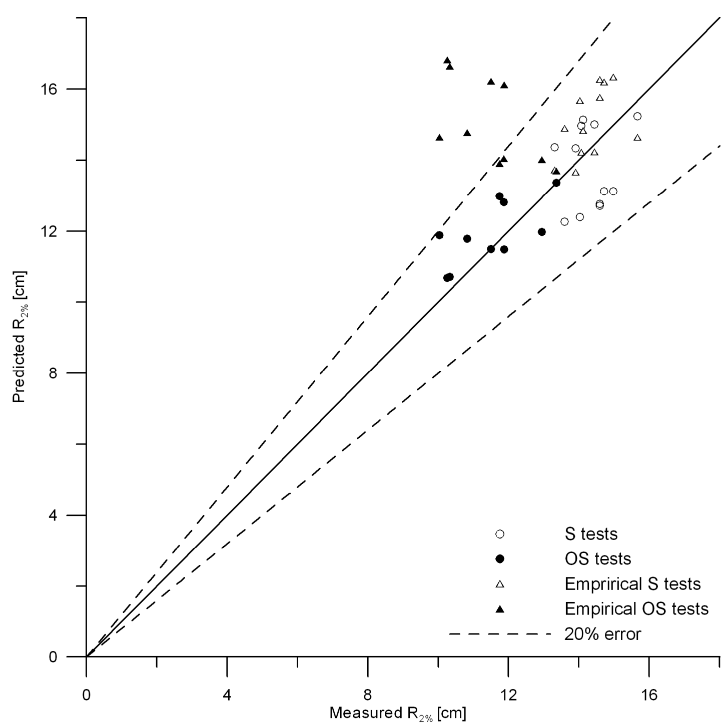

Fig. 37: Measured and predicted 2% runup heights $R_{2\%}$ for S and OS tests.

4.3 SEEPAGE AND OVERTOPPING RATES

Fig. 38 compares the measured and predicted rates of q_{os} where q_o and q_s were not measured separately. For the S tests, the predicted overtopping rate q_o is zero or negligible in comparison with the predicted seepage rate q_s. For the OS tests, the ratio between the predicted q_s and q_o is in the range of 0.2 – 0.9 except for test RO20C1 with negligible q_o and q_s as shown in Table 8. The seepage rate q_s is relatively small but not negligible. The numerical model predicts q_{os} within the factor of about two partly because the present formulas for q_o and q_s are developed using the same tests. Fig. 38 also includes the overtopping rates predicted by the empirical formula of Van der Meer and Janssen (1995). They proposed two different formulas for breaking and non-breaking waves. For the case of normally incident waves on a slope with no berm, these formulas can be expressed as

$$\begin{array}{llll} \text{Breaking waves} & \rightarrow & Q_b = 0.06\exp\left(-5.2R_b\right) & \text{if} \quad \xi<2 \\ \text{Non-breaking waves} & \rightarrow & Q_n = 0.2\exp\left(-2.6R_n\right) & \text{if} \quad \xi>2 \end{array} \tag{24}$$

with

$$Q_b = \frac{q_o}{\sqrt{gH_{1/3}^3}}\sqrt{\frac{s_{op}}{\tan\theta}}; \quad R_b = \frac{R_c}{H_{1/3}}\frac{\sqrt{s_{op}}}{\tan\theta}\frac{1}{\gamma_f\gamma_h}; \quad Q_n = \frac{q_o}{\sqrt{gH_{1/3}^3}}; \quad R_n = \frac{R_c}{H_{1/3}}\frac{1}{\gamma_f\gamma_h} \tag{25}$$

$$\xi = \left(\frac{gT_p^2}{2\pi H_{1/3}}\right)^{0.5}\tan\theta; \quad s_{op} = \frac{2\pi H_{1/3}}{gT_p^2}; \quad \gamma_h = 1-0.03\left(4-\frac{d_t}{H_{1/3}}\right)^2 \quad \text{if} \quad \frac{d_t}{H_{1/3}} < 4 \tag{26}$$

where Q_b and $Q_n =$ dimensionless overtopping rate for breaking and non-breaking waves, respectively; $q_o =$ overtopping rate; $H_{1/3}$ = significant wave height at the toe of the slope; $s_{op} =$ wave steepness; ξ = surf similarity parameter; R_b and $R_n =$ dimensionless crest height for breaking and non-breaking waves, respectively; $R_c =$ crest height above SWL; γ_f = reduction factor due to slope roughness; γ_h = reduction factor due to wave breaking on a shallow foreshore which is less than unity if $\left(d_t / H_{1/3}\right) < 4$, with d_t = toe depth. The reduction factor γ_f is taken as γ_f = 0.52. The significant wave height $H_{1/3}$ for each test is obtained from the time series of the free surface elevation measured by the wave gauge at the toe of the slope. All the parameters used for the estimation of the overtopping rate for each test are summarized in Table 9 and Table 10 together with the measured q_{os}.

Fig. 38 shows that the empirical formula can not predict the seepage rate q_s and overpredicts the overtopping rate for the wide permeable crest of the OS tests considerably, essentially because infiltration effects on the permeable crests are not accounted for.

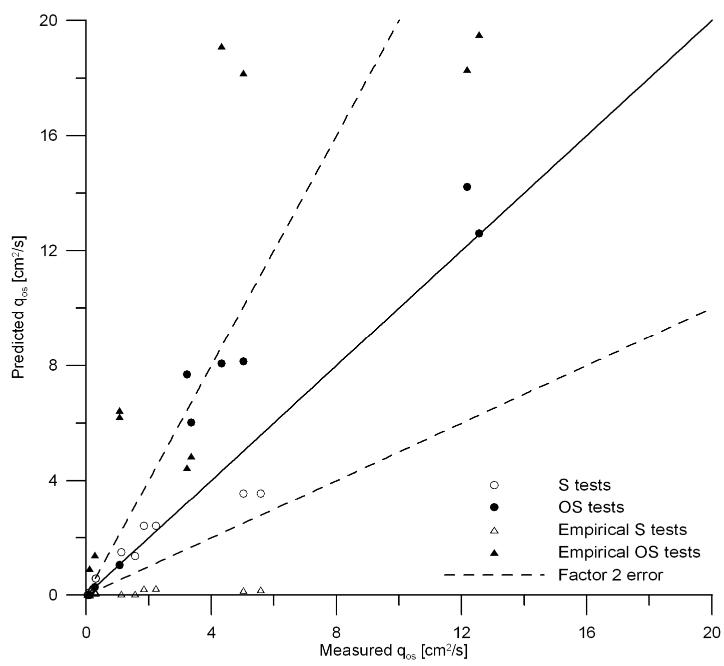

Fig. 38: Measured and predicted q_{os} for S and OS tests.

Table 8: Ratio between the predicted q_s and q_o for OS tests.

Test	Predicted				Measured
	q_o [cm²/s]	q_s [cm²/s]	q_{os} [cm²/s]	q_s / q_o	q_{os} [cm²/s]
RO20B1	0.19	0.10	0.29	0.54	0.28
RO20C1	0.01	0.00	0.01	0.00	0.11
RO22B1	4.91	1.12	6.03	0.23	3.36
RO22B2	6.44	1.24	7.68	0.19	3.22
RO22C1	0.56	0.50	1.06	0.89	1.07
RO22C2	0.55	0.50	1.05	0.90	1.07
RO24B1	12.07	2.15	14.22	0.18	12.18
RO24B2	10.45	2.14	12.60	0.21	12.56
RO24C1	6.29	1.78	8.07	0.28	4.33
RO24C2	6.37	1.78	8.15	0.28	5.02

Table 9: Comparison with empirical formula for overtopping rates for S tests.

Test	$H_{1/3}$ $[cm]$	T_p $[s]$	R_c $[cm]$	ξ	γ_h	R_b, R_n	Q_b, Q_n	Empirical q_o $\left[cm^2/s\right]$	Measured q_{os} $\left[cm^2/s\right]$
RS20B1	14.90	2.3	18.6	1.5	0.79	2.03	0.000002	0.01	0.12
RS20B2	14.59	2.3	18.6	1.5	0.80	2.04	0.000001	0.01	0.10
RS20C1	11.09	3.0	18.6	2.3	0.86	3.75	0.000012	0.01	0.04
RS20C2	11.90	3.0	18.6	2.2	0.85	3.56	0.000019	0.02	0.05
RS22B1	15.56	2.3	16.6	1.5	0.81	1.75	0.000007	0.04	1.57
RS22B2	15.63	2.3	16.6	1.5	0.80	1.75	0.000007	0.04	1.13
RS22C1	12.09	2.9	16.6	2.1	0.86	3.06	0.000070	0.09	0.31
RS22C2	11.58	2.9	16.6	2.1	0.87	3.16	0.000054	0.07	0.30
RS24B1	16.91	2.3	14.6	1.4	0.81	1.48	0.000028	0.19	5.57
RS24B2	15.95	2.3	14.6	1.4	0.82	1.50	0.000025	0.16	5.02
RS24C1	11.77	2.9	14.6	2.1	0.89	2.69	0.000188	0.24	2.23
RS24C2	11.64	2.9	14.6	2.1	0.89	2.70	0.000177	0.22	1.84

Table 10: Comparison with empirical formula for overtopping rates for OS tests.

Test	$H_{1/3}$ $[cm]$	T_p $[s]$	R_c $[cm]$	ξ	γ_h	R_b, R_n	Q_b, Q_n	Empirical q_o $\left[cm^2/s\right]$	Measured q_{os} $\left[cm^2/s\right]$
RO20B1	14.45	2.3	9.7	1.5	0.80	1.06	0.000239	1.40	0.28
RO20C1	10.19	3.0	9.7	2.4	0.88	2.08	0.000905	0.92	0.11
RO22B1	14.42	2.3	7.7	1.5	0.82	0.82	0.000833	4.86	3.36
RO22B2	13.80	2.3	7.7	1.6	0.83	0.83	0.000799	4.46	3.22
RO22C1	12.03	2.9	7.7	2.1	0.86	1.42	0.004927	6.44	1.07
RO22C2	11.94	2.9	7.7	2.1	0.87	1.43	0.004819	6.22	1.07
RO24B1	15.69	2.3	5.7	1.5	0.82	0.58	0.002886	18.30	12.18
RO24B2	16.30	2.3	5.7	1.4	0.81	0.58	0.002961	19.51	12.56
RO24C1	12.25	2.9	5.7	2.1	0.88	1.02	0.014227	19.11	4.33
RO24C2	12.08	2.9	5.7	2.1	0.88	1.03	0.013829	18.18	5.02

4.4 OVERTOPPING RATES FOR O TESTS

Fig. 39 shows the measured and predicted values of the wave overtopping probability P_o and the normalized overtopping rate q_o/q_{SWL} for the O tests with $q_s = 0$ where P_o and q_o were measured for each test. The measured q_o for each test is normalized by the predicted q_{SWL} for the same test. The solid line in Fig. 39 corresponds to Eq. (17) with $a = 0.6$ and $b = 1.5$ where $a = 0.57 – 0.67$ and $b = 1.40 – 1.57$ for the 12 O tests. Fig. 39 shows that Eq. (17) represents the measured relationship between P_o and q_o fairly well. However, the numerical model predicts the wider range of P_o than the measured range of P_o because the measured P_o varied less with the crest height R_c than the variation predicted by Eq. (4). The wider variation of P_o leads to the wider variation of the predicted q_o/q_{SWL} in Fig. 39. Consequently, the accurate prediction of q_o requires the accurate prediction of P_o because q_o is sensitive to P_o in Eq. (17).

The accurate prediction of P_o using Eqs. (2) and (4) requires the reliable estimates of $R_{1/3}$ and $\overline{\eta_r}$ where $R_{1/3}$ depends on σ_r and $\overline{\eta_r}$ in Eq. (5). The predicted values of $\overline{\eta_r}$, σ_r and $R_{1/3}$ depend somewhat on the runup wire height δ_r discussed in relation to Eq. (16) and the breaker ratio parameter γ in the formula by Battjes and Stive (1985) for the energy dissipation rate D_B due to wave breaking in Eq.(6). For the S and OS tests, $\delta_r = 2$ cm and use is made of $\gamma = 0.7$ calibrated in the previous comparisons by Kobayashi et al. (2006a, b). For the O tests, no runup wire was deployed and no measurement was made of the wave transformation on the beach in front of the revetment with the 1/2 slope in Fig. 3. Consequently, the sensitivity of the predicted $\overline{\eta_r}$, σ_r, $R_{1/3}$, P_o and q_o to $\delta_r = 1 – 2$ cm and $\gamma = 0.7 – 0.9$ is examined as discussed in the following section.

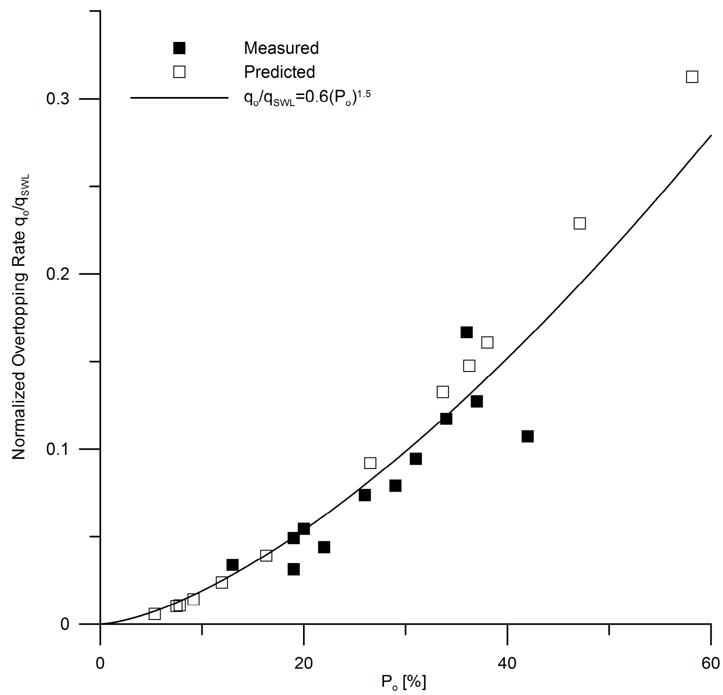

Fig. 39: Measured and predicted overtopping probability P_o vs. normalized overtopping rate q_o / q_{SWL} for overtopping (O) tests.

4.4.1 SENSITIVITY TO γ AND δ_r

Table 11 shows the predicted values of $\overline{\eta_r}$, σ_r and $R_{1/3}$ obtained for the runup wire height $\delta_r = 1-2$ cm and the breaker ratio parameter $\gamma = 0.7-0.9$. The predicted values of $\overline{\eta_r}$ increase about 20% with the increase of the breaker ratio parameter from $\gamma = 0.7$ to $\gamma = 0.9$, while the effect of the decrease of $\delta_r = 2$ cm to $\delta_r = 1$ cm is much bigger, resulting in about 100% increase for $\overline{\eta_r}$. On the other hand, σ_r is much less sensitive to γ and δ_r, with differences of 10 - 20% where σ_r is more sensitive to γ. The increase of about 15 - 20% for the predicted $R_{1/3}$ results from the decrease of δ_r and the increase of γ. The uncertainties related to γ and δ_r, are on the same order of magnitude for the accuracy of the present numerical model.

Table 12, Fig. 40 and Fig. 41 show very clearly that the increase of the predicted P_o and q_o is amplified because of their sensitivity to $\overline{\eta_r}$, σ_r and $R_{1/3}$.

It is noted that the predicted P_o and q_o in Fig. 39 are based on δ_r = 1 cm and γ = 0.9 to improve the agreement with the data. In short, the relatively small error or uncertainty of $\overline{\eta_r}$, σ_r and $R_{1/3}$ will result in the large error or uncertainty of P_o and q_o.

Table 11: Predicted $\overline{\eta_r}, \sigma_r$ and $R_{1/3}$ with $\delta_r = 1-2$ cm and $\gamma = 0.7-0.9$ for O tests.

Test	**Predicted $\overline{\eta_r}$ [cm]**			**Predicted σ_r [cm]**			**Predicted $R_{1/3}$ [cm]**		
	$\delta_r = 2$ $\gamma = 0.7$	$\delta_r = 2$ $\gamma = 0.9$	$\delta_r = 1$ $\gamma = 0.9$	$\delta_r = 2$ $\gamma = 0.7$	$\delta_r = 2$ $\gamma = 0.9$	$\delta_r = 1$ $\gamma = 0.9$	$\delta_r = 2$ $\gamma = 0.7$	$\delta_r = 2$ $\gamma = 0.9$	$\delta_r = 1$ $\gamma = 0.9$
A11A	1.26	1.56	2.75	2.99	3.57	3.70	8.73	10.48	12.00
A12A	1.16	1.47	2.63	2.77	3.39	3.52	8.09	9.93	11.42
A21A	1.32	1.65	2.84	3.03	3.65	3.77	8.91	10.76	12.27
A22A	1.29	1.66	2.83	2.85	3.52	3.64	8.42	10.47	11.94
B12A	1.23	1.55	2.72	2.90	3.50	3.62	8.47	10.30	11.77
B22A	1.37	1.75	2.94	2.99	3.66	3.76	8.84	10.89	12.35
C11A	1.49	1.83	3.05	3.30	3.89	3.99	9.74	11.55	13.03
C12A	1.34	1.68	2.88	3.05	3.66	3.77	8.96	10.83	12.29
C21A	1.52	1.87	3.09	3.32	3.92	4.02	9.82	11.67	13.15
C22A	1.47	1.87	3.08	3.13	3.81	3.90	9.31	11.39	12.83
D12A	1.39	1.72	2.92	3.14	3.73	3.83	9.25	11.05	12.50
D22A	1.53	1.92	3.14	3.24	3.90	3.98	9.64	11.66	13.08
A11A	1.26	1.56	2.75	2.99	3.57	3.70	8.73	10.48	12.00
A12A	1.16	1.47	2.63	2.77	3.39	3.52	8.09	9.93	11.42

Table 12: Measured and predicted P_o and q_o with $\delta_r = 1-2$ cm and $\gamma = 0.7-0.9$ for O tests.

Test	P_o [%]				q_o [cm^2/s]			
	Data	$\delta_r = 2$ $\gamma = 0.7$	$\delta_r = 2$ $\gamma = 0.9$	$\delta_r = 1$ $\gamma = 0.9$	Data	$\delta_r = 2$ $\gamma = 0.7$	$\delta_r = 2$ $\gamma = 0.9$	$\delta_r = 1$ $\gamma = 0.9$
A11A	22.0	0.5	3.1	7.8	1.760	0.004	0.100	0.430
A12A	19.0	0.2	1.9	5.4	1.860	0.001	0.044	0.218
A21A	19.0	0.7	3.8	9.2	1.290	0.006	0.147	0.586
A22A	13.0	0.3	3.0	7.5	1.370	0.002	0.100	0.420
B12A	26.0	0.9	4.9	11.9	2.900	0.011	0.245	0.934
B22A	20.0	1.4	7.3	16.3	2.300	0.023	0.490	1.650
C11A	42.0	6.2	17.9	36.3	4.790	0.341	2.440	6.595
C12A	34.0	3.3	12.3	26.5	4.890	0.115	1.258	3.828
C21A	29.0	6.6	19.0	38.0	3.580	0.376	2.693	7.288
C22A	31.0	4.4	16.6	33.7	4.200	0.192	2.108	5.885
D12A	36.0	8.3	23.5	47.1	7.100	0.546	3.654	9.738
D22A	37.0	10.8	31.1	58.2	5.800	0.864	6.041	14.241

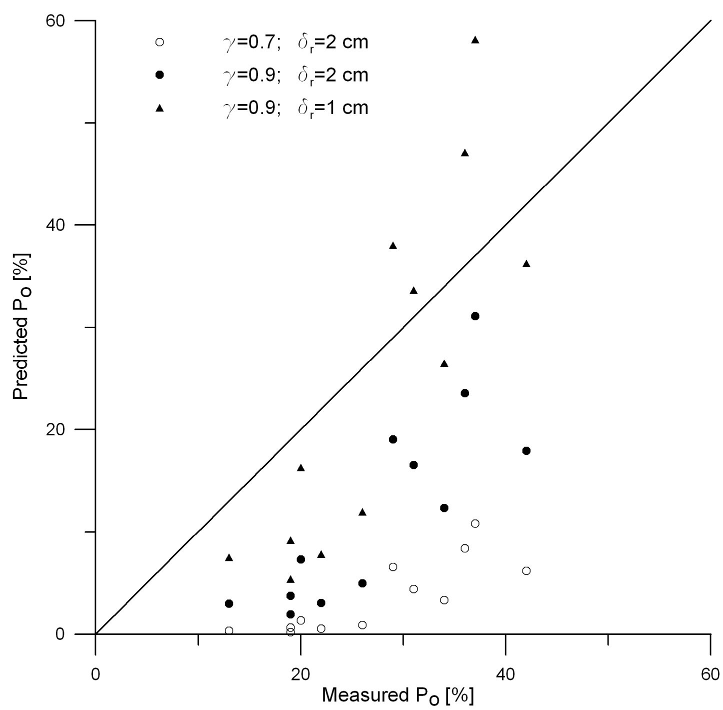

Fig. 40: Sensitivity of P_o to breaker ratio parameter γ and runup wire height δ_r for O tests.

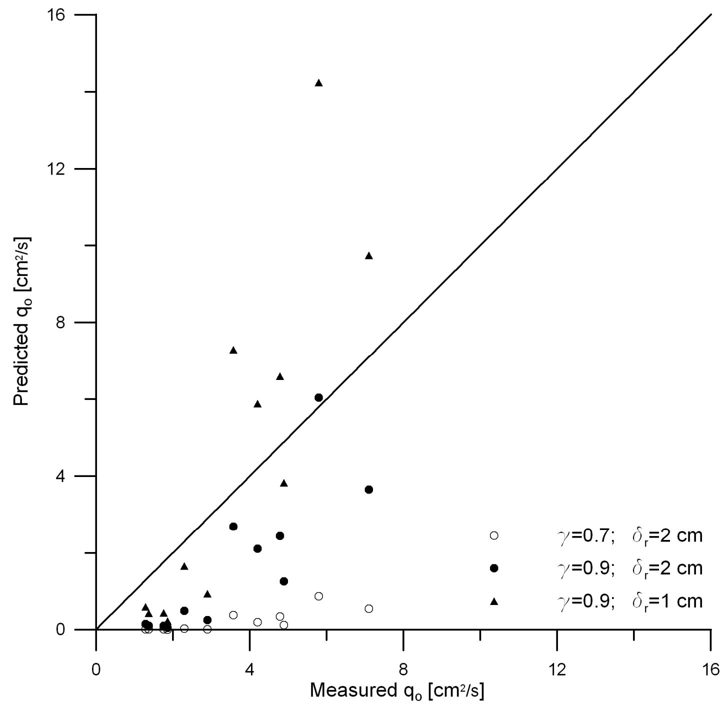

Fig. 41: Sensitivity of q_o to breaker ratio parameter γ and runup wire height δ_r for O tests

4.5 POROUS LAYER EFFECTS

To examine the permeability effects on q_{os}, computation is also made for the OS tests with no permeable layer by specifying $z_p = z_b$ and $h_p = 0$. Fig. 42 compares the predicted values of q_{os} for the porous and impermeable slopes. As expected, the predicted values of q_o for the impermeable slope are much bigger than q_{os} for the porous slope. The increase of the predicted overtopping rate is caused essentially by the fact that the normalized infiltration width L_* in Eq. (18) is zero. Moreover, the energy dissipation rate due to porous flow resistance is zero and the wave-induced onshore flux q_{SWL} at the still water shoreline is larger for $L_* = 0$, $a = 1$, $b = 1$ and $q_o = P_o \cdot q_{SWL}$. No experiment was conducted for the impermeable slope and the results for Fig. 42 need to be verified.

Fig. 43 compares the computed cross-shore variations of $\bar{\eta}$, σ_η, $\bar{u}$ and σ_u for test RO24B1 on the porous and impermeable slopes. As observed by de los Santos and Kobayashi (2005) the permeability effects on the slope are smaller than expected. The main difference is that the mean horizontal velocity $\bar{u}$ increases significantly on the impermeable slope due to the increase of q_{os} in the continuity equation (10).

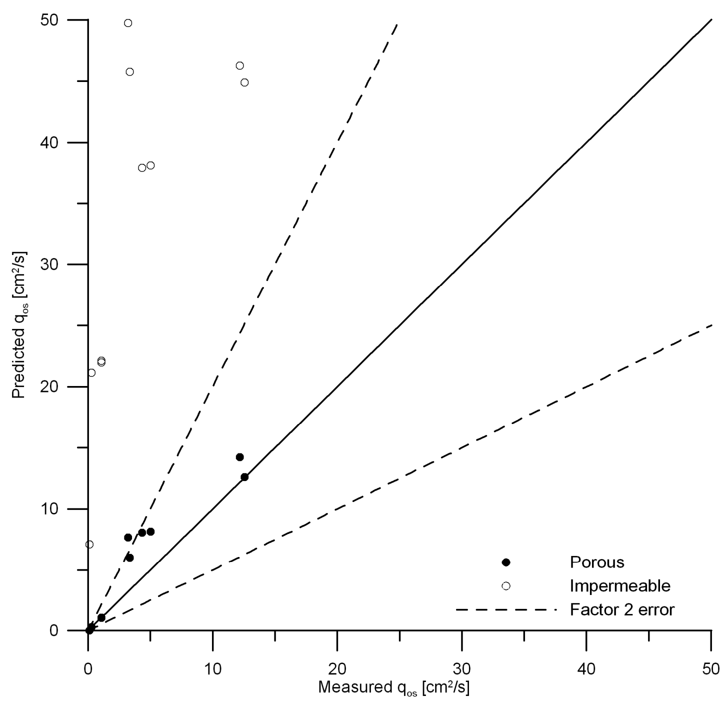

Fig. 42: Permeability effects on predicted q_{os} for all OS tests.

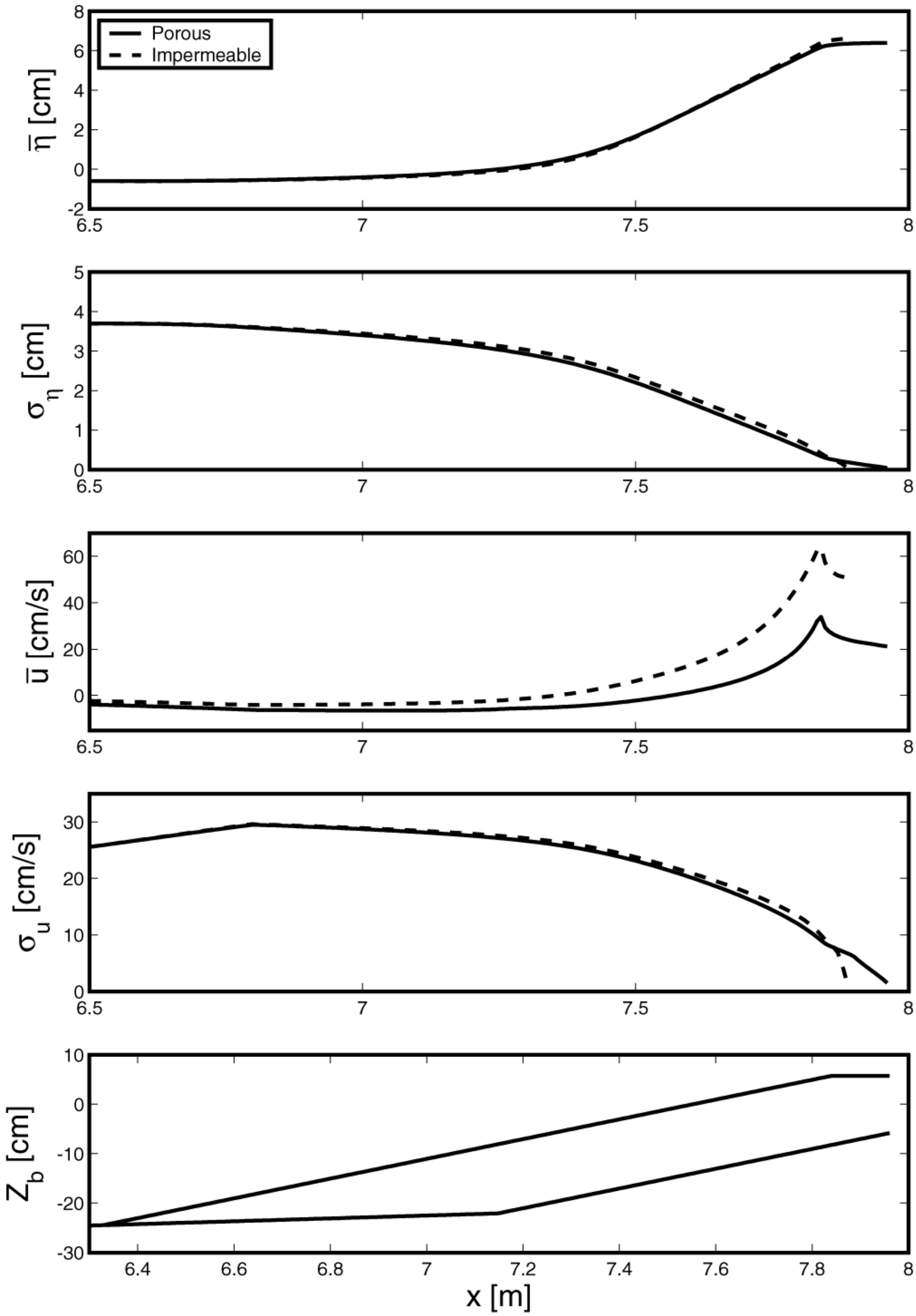

Fig. 43: Permeability effects on $\overline{\eta}$, σ_η, $\overline{u}$ and σ_u for test RO24B1.

4.6 REFLECTION COEFFICIENT

Fig. 44 compares the measured and predicted reflection coefficients. The reflection coefficient r predicted using Eq. (15) is not sensitive to the values of δ_r. The numerical model overpredicts r for the S and OS tests with the 1/5 slope and underpredicts r for the O tests with the 1/2 slope. This trend is the same as found by Kobayashi et al. (2006a) for the case of no seepage and no overtopping. Wave reflection may need to be included in the momentum and energy equations (6) and the continuity equation (10) in future.

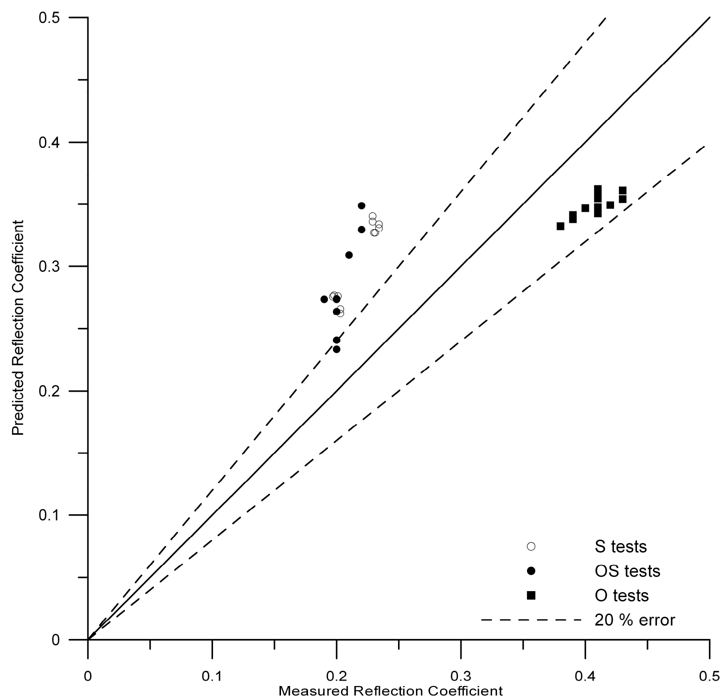

Fig. 44: Measured and predicted wave reflection coefficients for S, OS and O tests.

CHAPTER 5 CONCLUSIONS

Experiments were conducted in a wave flume to investigate wave seepage and overtopping of permeable slopes with wide crests. The time-averaged numerical model for irregular wave transmission and runup is extended to include the landward water flux due to wave seepage and overtopping. The measured wave runup distributions are shown to be represented by the Weibull distribution whose shape parameter increases with the increase of the wave overtopping probability. The Weibull distribution reduces to the widely-used Rayleigh distribution for minor overtopping. The wave overtopping rate normalized by the wave-induced water flux at the still water shoreline is expressed as a function of the wave overtopping probability with the two empirical parameters related to infiltration which depend essentially on the horizontal number of stones above the maximum wave setup on the seaward slope. The normalized overtopping rate is shown to be very sensitive to the degree of infiltration. The seepage flow driven by the wave setup on the permeable slope is analyzed to obtain a simple formula for the seepage rate.

The extended numerical model coupled with the formulas for the seepage and overtopping rates is shown to be in agreement with the cross-shore variations of the mean and standard deviation of the measured free surface elevation and cross-shore fluid velocity. The effect of the water flux due to wave seepage and overtopping is practically limited to the mean cross-shore velocity. The numerical model predicts the significant and 2% runup heights within an error of 20% and the combined overtopping and seepage rate within a factor of two. The seepage rate is found to be comparable with the overtopping rate even for the case of significant overtopping. The prediction of the wave reflection coefficient is less satisfactory because the numerical model does not include the effects of reflected waves in the continuity, momentum and energy equations.

The time-averaged numerical model for wave overtopping and seepage is much more efficient computationally but more empirical than time-dependent numerical models (e.g., Kobayashi and Raichle 1994). The proposed numerical model will need to be calibrated and evaluated using more extensive data sets including field data. Furthermore, detailed measurements of the overtopping and seepage flows will be necessary in order to refine the simple formulas for the overtopping and seepage rates.

REFERENCES

Allan, J.C. and Komar, P.D. (2002). "A dynamic revetment and artificial dune for shore protection." *Coastal Engineering 2002*, *Proc. 28th Coastal Engineering Conf.,* World Scientific, Singapore, 2044-2056.

Battjes, J.A. and Stive, M.J.F., (1985). "Calibration and verification of a dissipation model for random breaking waves." *J. Geophys. Res.*, 90(C5), 9159-9167.

de los Santos, F.J. and Kobayashi, N. (2005). "Irregular wave setup and runup on cobble beaches and revetments." *Research Rep. No. CACR-05-06*, Center for Applied Coastal Research, University of Delaware, Newark, Del.

de los Santos, F.J., Kobayashi, N. and Losada, M.A. (2006). "Irregular wave runup and overtopping on revetments and cobble beaches." *Coastal Engineering 2006, Proc. 30th Coastal Engineering Conf.*, World Scientific, Singapore. (accepted)

Kobayashi, N., Cox, D.T. and Wurjanto, A. (1990). "Irregular wave reflection and run-up on rough impermeable slopes." *J. Waterw., Port, Coastal, Ocean Eng.*, 116(6), 708-726.

Kobayashi, N. and de los Santos, F.J. (2006). "Irregular wave seepage and overtopping of permeable slopes." *J. Waterw., Port, Coastal, Ocean Eng.* (submitted).

Kobayashi, N., de los Santos, F.J. and Kearney, P.G. (2006a). "Time-averaged probabilistic model for irregular wave runup on permeable slopes." *J. Waterw., Port, Coastal, Ocean Eng.* (under review).

Kobayashi, N., Meigs, L.E., Ota, T. and Melby, J.A. (2006b). "Irregular breaking wave transmission over submerged porous breakwater." *J. Waterw., Port, Coastal, Ocean Eng.* (in press).

Kobayashi, N. and Raichle, A.W. (1994). "Irregular wave overtopping of revetments in surf zones." *J. Waterw., Port, Coastal, Ocean Eng.,* 120(1), 56-73.

Kobayashi, N., Zhao, H. and Tega, Y. (2005). "Suspended sand transport in surf zones." *J. Geophys. Res.*, 110, C12009, doi:10.1029/2004JC002853.

Pozueta, B., Van Gent, M.R.A. and Van den Boogaard, H. (2004). "Neural network modelling of wave overtopping at coastal structures." *Coastal Engineering 2004*, *Proc. 29th Coastal Engineering Conf.,* World Scientific, Singapore, 4275-4287.

Steendam, G.J., Van der Meer, J.W., Verhaeghe, H., Besley, P., Franco, L. and Van Gent, M.R.A. (2004). The international database on wave overtopping." *Coastal Engineering 2004*, *Proc. 29th Coastal Engineering Conf.,* World Scientific, Singapore, 4301-4313.

Troch, P., Geeraerts, J., Van de Walle, B., DeRouck, J., Van Damme, L., Allsop, W. and Franco, L. (2004). "Full-scale wave overtopping measurements on the Zeebrugge rubble mound breakwater." *Coastal Eng*., 51, 609-628.

Van der Meer, J.W. (1992). "Conceptual design of rubble mound breakwaters." *ICCE Proc., Short Course on Design and Reliability of Coastal Structures*, Technoprint, Bologna, Italy, 447-510.

Van der Meer, J.W. and Janssen, P.F.M. (1995). "Wave run-up and wave overtopping at dikes." *Wave forces on inclined and vertical wall structures,* ASCE. Reston, Va., 1-27.

Van Gent, M.R.A. (1995). "Porous flow through rubble-mound materials." *J. Waterw., Port, Coastal, Ocean Eng.*, 121(3), 176-181.

Verhagen, H.J., Steenaard, J. and Tuan, T.Q. (2004). "Infiltration of overtopping water in a breakwater crest." *Coastal Engineering 2004*, *Proc. 29th Coastal Engineering Conf.,* World Scientific, Singapore, 4253-4262.

Zanuttigh, B. and Lamberti, A. (2006). "Experimental analysis and numerical simulations of waves and current flows around low-crested rubble-mound structures." *J. Waterw., Port, Coastal, Ocean Eng.*, 132(1), 10-27.